# Simplified CSP Analysis of a Stiff Stochastic ODE System

M. Salloum[a], A. Alexanderian[b], O. Le Maître[c], H.N. Najm[a], O.M. Knio[b]

[a] *Sandia National Laboratories, Livermore, CA 94551*
[b] *Department of Mechanical Engineering, The Johns Hopkins University, Baltimore, MD 21218-2686*
[c] *LIMSI-CNRS, F-91403 Orsay, France*

**Abstract**

We develop a simplified computational singular perturbation (CSP) analysis of a stochastic dynamical system. We focus on the case of parametric uncertainty, and rely on Polynomial Chaos (PC) representations to quantify its impact. We restrict our attention to a system that exhibits distinct timescales, and that tends to a deterministic steady state irrespective of the random inputs. A detailed analysis of eigenvalues and eigenvectors of the stochastic system Jacobian is conducted, which provides a relationship between the PC representation of the stochastic Jacobian and the Jacobian of the Galerkin form of the stochastic system. The analysis is then used to guide the application of a simplified CSP formalism that is based on relating the slow and fast manifolds of the uncertain system to those of a nominal deterministic system. Two approaches are specifically developed with the resulting simplified CSP framework. The first uses the stochastic eigenvectors of the uncertain system as CSP vectors, whereas the second uses the eigenvectors of the nominal system as CSP vectors. Numerical experiments are conducted to demonstrate the results of the stochastic eigenvalue and eigenvector analysis, and illustrate the effectiveness of the simplified CSP algorithms in addressing the stiffness of the system dynamics.

## 1. Introduction

Modeling complex dynamical systems often involves solving large systems of ordinary differential equations (ODEs). In many cases, the time scales in such systems span several orders of magnitude, and the mathematical models are thus deemed to be "stiff". Stiffness is specifically associated with the large range of amplitudes of the negative real system eigenvalues. Stability issues are encountered when integrating such systems using explicit methods, where it is necessary that the time step be limited to very small values. Alternatively, implicit methods can be used, allowing larger time steps, but with larger per time-step cost, and complexity of the time integration method. Therefore, it is generally useful to reduce stiffness of these systems to enable their efficient explicit time integration and analysis of their dynamics.

Computational singular perturbation (CSP) [21, 13] has been found to be an effective tool for analysis of stiff ODE systems, allowing model reduction and mitigating stiffness. CSP relies on the identification of a set of vectors/co-vectors that provide suitable decoupling of fast and slow processes. This allows the identification of fast exhausted modes, and the associated set of algebraic constraints defining the slow invariant manifold (SIM) along which the solution evolves according to the slow time scales. This information allows detailed and precise analysis of the dynamics, providing cause-and-effect insights, and key information for model reduction. Given a $1/\epsilon$ separation between fast and slow time scales, the eigenvectors of the ODE Jacobian matrix provide an $O(\epsilon)$ approximation of the ideal CSP vectors. Higher-order constructions are available, employing an iterative refinement procedure. In particular, the CSP methodology has been used extensively for analysis and model reduction in ODEs resulting from chemical systems [19, 21, 13, 20, 22, 12, 8, 40, 28, 43, 14, 41, 39, 38, 18, 29].

*Email addresses:* mnsallo@sandia.gov (M. Salloum), aalexa20@jhu.edu (A. Alexanderian), olm@limsi.fr (O. Le Maître), hnnajm@sandia.gov (H.N. Najm), knio@jhu.edu (O.M. Knio)

*To appear in Computer Methods in Applied Mechanics and Engineering* *January 25, 2012*

Heuristic methods for model reduction based on CSP analysis have been demonstrated in strongly nonlinear dynamical systems, in particular chemical models of complex hydrocarbon fuels, with significant degrees of stiffness. The methodology enables a choice among a range of reduced models of varying complexity, depending on user-specified tolerances. However, these model reduction methods have not been extended to situations in which the starting, detailed, dynamical model has some degree of uncertainty, whether in its structure or parameters/initial conditions. This extension is highly relevant, as complex dynamical systems frequently involve uncertainty, and it is intuitively clear that the degree of uncertainty in the detailed model and the meaningful degree of model reduction are inter-related. There has been very little work in this area. We may cite the work in [34] where POD model reduction methods were analyzed in the context of small and linear perturbations to model parameters. To our knowledge, there is no work on model reduction strategies for uncertain dynamical systems, allowing for large degrees of uncertainty and requiring stochastic uncertainty quantification methods.

Uncertainty quantification (UQ) methods have been used in order to assess the effect of different sources of uncertainty on dynamical system behavior. As the system size increases, the number of sources of uncertainty often increases leading to a significant increase in computational complexity. For example, the combustion of complex hydrocarbons may involve thousands of elementary reactions whose kinetic parameters are poorly characterized. Accounting for uncertainty in all these parameters is a signficant challenge, even presuming well characterized parametric uncertainties. Global sensitivity analysis may be used to cut down the number of uncertain parameters of significance, however this analysis in itself requires large computational effort and the residual UQ problem remains a significant challenge.

Polynomial chaos (PC) spectral UQ methods [11, 25, 27, 47, 35, 48, 26, 6, 24] have been introduced, and used over the past two decades, for alleviating the computational cost of Monte Carlo UQ methods, and to support uncertainty management and decision making analyses. PC methods have been extensively used for UQ in different physical problems such as fluid [25, 27, 31] and solid [11, 10] mechanics, and chemical reactions [35, 26, 32]. The essential goal in PC methods is to obtain a spectral representation of the variables of interest. This goal can be accomplished using two approaches. This first approach relies on computing a set of deterministic solutions for different realizations of the uncertain parameters then projecting these solutions on a spectral basis in order to recover a unique spectral representation of the solution of interest. This approach does not require the reformulation of the governing equations as it only requires the existence of a deterministic model. Hence this approach is often called "non-intrusive spectral projection" (NISP). In the second (intrusive) approach, known as the *Galerkin* method, the governing equations are reformulated based on the PC expansions of the random parameters and the variables. This results in an expanded system of differential equations that, once solved, yields a suitable representation of the stochastic variables.

In this paper, we propose to develop a new methodology that combines CSP and spectral PC uncertainty quantification methods for the analysis and reduction of multiscale problems under uncertainty. Our goal is to simultaneously analyze the stochastic system and efficiently integrate its dynamics. We focus our attention on an $n$-dimensional kinetic system, with uncertainty in initial conditions and rate parameters, and assume that the uncertainty can be parameterized in terms of a random input vector $\boldsymbol{\xi} \in \mathbb{R}^M$. The Galerkin formulation of such systems would result in an expanded system of $n(P+1)$ differential equations (see Section 2.4.2), where $P$ is the number of terms in the PC expansion of the solution variables. An obvious approach is to apply CSP directly to the Galerkin system. This would involve an analysis of the deterministic Jacobian of the Galerkin system (cf. Section 3), which we denote by $\mathcal{J}$. This deterministic Jacobian, $\mathcal{J}$, should be carefully distinguished from the Jacobian of the stochastic system, $J(\boldsymbol{\xi})$, which we refer to as the stochastic Jacobian. Clearly, $\mathcal{J}$ belongs to the space $\mathbb{R}^{n(P+1)\times n(P+1)}$, whereas each realization of the stochastic Jacobian, $J$, belongs to the space $\mathbb{R}^{n\times n}$.

While the application of CSP to the Galerkin reformulated system appears to be quite general, the approach entails the following challenges: (i) the Galerkin Jacobian, $\mathcal{J}$, may not be $\mathbb{R}$-diagonalizable even when it arises from the Galerkin projection of a stochastic problem with an almost surely $\mathbb{R}$-diagonalizable stochastic Jacobian (see [37] for notable exceptions in the context of hyperbolic systems); and (ii) the Galerkin Jacobians commonly exhibit eigenvalues with multiplicity greater than one, complicating the application of the CSP procedure.

To circumvent such difficulties, we explore the feasibility of applying a *simplified* CSP methodology. The

approach is specifically motivated by the question of assessing: *under what ranges of uncertainties in the model parameters would a deterministic reduced model remain valid or useful?* Assuming that this is feasible makes a simplified CSP procedure based on a spectral analysis of the stochastic Jacobian $J(\boldsymbol{\xi})$ possible. In this paper, we shall specifically explore this possibility. Of course, the approach is less general than the direct application of CSP to the Galerkin reformulated system. However, it appears to provide tangible advantages, including: (a) the direct and efficient characterization of the dependence of the *physical* fast and slow manifolds on the uncertainty term $\boldsymbol{\xi}$, (b) the potential of re-exploiting an available or legacy reduced model, originally obtained based on analyzing a deterministic (nominal) system, and (c) a more efficient algorithm. We shall specifically investigate the merits and properties of this simplified CSP approach in the context of a model kinetic system.

The structure of this paper is as follows. In section 2, we collect the basic notation and the background ideas used throughout the paper. The simplified CSP algorithm hinges on stochastic time scales and eigenvectors derived from the spectral analysis of $J(\boldsymbol{\xi})$, which is outlined in section 3. In section 4 we develop our proposed simplified CSP reduction mechanism for uncertain systems. In section 5, we introduce a simple 3-species model problem and derive its stochastic Galerkin form. Numerical studies are conducted in section 6 to test the accuracy and effectiveness of the proposed method. Finally, in section 7 we provide a few concluding remarks and possible directions for further work.

## 2. Background

In this section we fix the notation and collect background results used in the rest of the paper.

### *2.1. Basic notation*

In what follows $(\Omega, \mathcal{F}, \mu)$ denotes a probability space, where $\Omega$ is the sample space, $\mathcal{F}$ is an appropriate $\sigma$-algebra on $\Omega$, and $\mu$ is a probability measure. A real-valued random variable $\xi$ on $(\Omega, \mathcal{F}, \mu)$ is an $\mathcal{F}/\mathcal{B}(\mathbb{R})$-measurable mapping $\xi : (\Omega, \mathcal{F}, \mu) \to (\mathbb{R}, \mathcal{B}(\mathbb{R}))$, where $\mathcal{B}(\mathbb{R})$ denotes the Borel $\sigma$-algebra on $\mathbb{R}$. The space $L^2(\Omega, \mathcal{F}, \mu)$ denotes the Hilbert space of real-valued square integrable random variables on $\Omega$. For a random variable $\xi$ on $\Omega$, we write $\xi \sim \mathcal{N}(0, 1)$ to mean that $\xi$ is a standard normal random variable and we write $\xi \sim \mathcal{U}(a, b)$ to mean that $\xi$ is uniformly distributed on the interval $[a, b]$. We use the term *iid* for a collection of random variables to mean that they are independent and identically distributed.The distribution function [17, 46] of a random variable $\xi$ on $(\Omega, \mathcal{F}, \mu)$ is given by $F_\xi(x) = \mu(\xi \leq x)$ for $x \in \mathbb{R}$.

### *2.2. Uncertainty quantification and polynomial chaos*

In this paper, we consider dynamical systems with finitely many random parameters, parameterized by a finite collection of real-valued *iid* random variables $\xi_1, \ldots, \xi_M$ on $\Omega$. We let $\mathcal{V} = \sigma(\{\xi_i\}_1^M)$ and, disregarding any other sources of uncertainty, work in the space $(\Omega, \mathcal{V}, \mu)$. By $F_{\boldsymbol{\xi}}$ we denote the joint distribution function of the random vector $\boldsymbol{\xi} = (\xi_1, \ldots, \xi_M)^T$. Note that since the $\xi_j$ are *iid*, they share a common distribution function, $F$, and consequently $F_{\boldsymbol{\xi}}(\boldsymbol{x}) = \prod_{j=1}^{M} F(x_j)$ for $\boldsymbol{x} \in \mathbb{R}^M$. Let us denote by $\Omega^* \subseteq \mathbb{R}^M$ the image of $\Omega$ under $\boldsymbol{\xi}$, $\Omega^* = \boldsymbol{\xi}(\Omega)$, and by $\mathcal{B}(\Omega^*)$ the Borel $\sigma$-algebra on $\Omega^*$.

It is often convenient to work in the probability space $(\Omega^*, \mathcal{B}(\Omega^*), F_{\boldsymbol{\xi}})$ instead of the abstract probability space $(\Omega, \mathcal{V}, \mu)$. We denote the expectation of a random variable $X : \Omega^* \to \mathbb{R}$ by

$$\langle X \rangle = \int_{\Omega^*} X(\boldsymbol{s})\, dF_{\boldsymbol{\xi}}(\boldsymbol{s}).$$

The space $L^2(\Omega^*, \mathcal{B}(\Omega^*), F_{\boldsymbol{\xi}})$, which we sometimes simply denote by $L^2(\Omega^*)$, is endowed with the inner product $(\cdot, \cdot) : L^2(\Omega^*) \times L^2(\Omega^*) \to \mathbb{R}$ given by

$$(X, Y) = \int_{\Omega^*} X(\boldsymbol{s}) Y(\boldsymbol{s})\, dF_{\boldsymbol{\xi}}(\boldsymbol{s}) = \langle XY \rangle .$$

In the case $\xi_i \overset{iid}{\sim} \mathcal{N}(0,1)$, any $X \in L^2(\Omega^*, \mathcal{B}(\Omega^*), F_{\boldsymbol{\xi}})$ admits an expansion of form,

$$X = \sum_{k=0}^{\infty} c_k \Psi_k, \tag{1}$$

where $\Psi_k$ are $M$-variate Hermite polynomials [1], and the series converges in $L^2(\Omega^*, \mathcal{B}(\Omega^*), F_{\boldsymbol{\xi}})$ sense:

$$\lim_{P\to\infty} \int_{\Omega^*} \left| X(\boldsymbol{s}) - \sum_{k=0}^{P} c_k \Psi_k(\boldsymbol{s}) \right|^2 dF_{\boldsymbol{\xi}}(\boldsymbol{s}) = 0.$$

The expansion (1) is known as the (Wiener-Hermite) polynomial chaos expansion [45, 5, 16, 24] of $X$. The polynomials $\{\Psi_k\}_0^\infty$ are orthogonal,

$$(\Psi_k, \Psi_l) = \langle \Psi_k \Psi_l \rangle = \delta_{kl} \left\langle \Psi_k^2 \right\rangle, \tag{2}$$

where $\delta_{kl}$ is the Kronecker delta.

Depending on the distributions appearing in the problem it is convenient to adopt alternative parameterizations and polynomial bases. For example, in the case $\xi_i \overset{iid}{\sim} \mathcal{U}(-1,1)$, we will use $M$-variate Legendre polynomials for the basis $\{\Psi_k\}_0^\infty$, and the expansion in (1) is a Generalized Polynomial Chaos [47] expansion of $X$. It is also possible to use $\xi_i$ that are independent but not necessarily identically distributed, which leads to a mixed polynomial chaos basis (cf. [24] for examples).

Finally, in practical computations, we will be approximating $X(\boldsymbol{\xi})$ with a truncated series,

$$X(\boldsymbol{\xi}) \approx \sum_{k=0}^{P} c_k \Psi_k(\boldsymbol{\xi}), \tag{3}$$

where $P$ is finite and depends on the truncation strategy adopted. In the following, we shall consider truncations based on the total degree of the retained polynomials in the series, such that $P$ is a function of the stochastic dimension $M$ and expansion "order" $p$ according to [24]:

$$1 + P = \frac{(M+p)!}{M!p!}. \tag{4}$$

Here $p$ refers to the largest polynomial degree in the expansion.

### *2.3. The approximation space $\mathcal{V}^p$*

Let us denote by $\mathcal{V}^p$, the subspace of $L^2(\Omega^*)$ spanned by $\{\Psi_0, \Psi_1, \ldots, \Psi_P\}$ with $P$ given by (4). Every element of $\mathcal{V}^p$ is a linear combination of $\{\Psi_j\}_0^P$. Random variables in $L^2(\Omega^*)$ will be approximated by elements in $\mathcal{V}^p$. The definition of the approximations in $\mathcal{V}^p$ of an element $u \in L^2(\Omega^*)$ will vary from one case to another; specifically, we shall rely on orthogonal projection of $u$ into $\mathcal{V}^p$ or on the Galerkin projection definition when the random variable $u$ is solution of an equation (or of a set of equations); see Section 2.4.2. The orthogonal projection allows us to define operations between elements of $\mathcal{V}^p$ in a rather straightforward way. For example, given $u, v \in \mathcal{V}^p$, we note that the product $(uv)$ is in general not in $\mathcal{V}^p$, but can be projected into $\mathcal{V}^p$ easily as follows [24]. Given,

$$u = \sum_{k=0}^{P} u^k \Psi_k, \quad v = \sum_{k=0}^{P} v^k \Psi_k,$$

the projection $w$ of $(uv)$ into $\mathcal{V}^p$ is

$$w = \sum_{k=0}^{P} w^k \Psi_k, \qquad w^k = \frac{1}{\langle \Psi_k^2 \rangle} \sum_{i=0}^{P} \sum_{j=0}^{P} u^i v^j \langle \Psi_i \Psi_j \Psi_k \rangle . \tag{5}$$

The function $w$ defined as in (5) is the product of $u$ and $v$ in $\mathcal{V}^p$; we denote this $\mathcal{V}^p$ product by

$$w = u \circledast v.$$

In the current work, we are also interested in random $n$-vectors $\boldsymbol{u}$ with components $u_i \in \mathcal{V}^p$ for $i = 1, \ldots, n$. In this case we write$\boldsymbol{u} \in (\mathcal{V}^p)^n$. Any $\boldsymbol{u} \in (\mathcal{V}^p)^n$ has a spectral representation,

$$\boldsymbol{u} = \sum_{k=0}^{P} \boldsymbol{u}^k \Psi_k,$$

with $\boldsymbol{u}^k \in \mathbb{R}^n$. We denote by $[\boldsymbol{u}]$ the $n(P+1)$-dimensional vector

$$[\boldsymbol{u}] = \begin{pmatrix} \boldsymbol{u}^0 \\ \boldsymbol{u}^1 \\ \vdots \\ \boldsymbol{u}^P \end{pmatrix},$$

and view $[\boldsymbol{u}]$ as the vector of "coordinates" of $\boldsymbol{u}$ in $(\mathcal{V}^p)^n$. We can also define operations between random $n$-vectors. For example, if $\boldsymbol{v} \in (\mathcal{V}^p)^n$ has a spectral representation,

$$\boldsymbol{v} = \sum_{k=0}^{P} \boldsymbol{v}^k \Psi_k,$$

then the dot product of $\boldsymbol{u}$ and $\boldsymbol{v}$, $\alpha = \boldsymbol{u} \cdot \boldsymbol{v}$, can be projected into $\mathcal{V}^p$ easily as follows:

$$\alpha = \sum_{k=0}^{P} \alpha^k \Psi_k, \qquad \alpha^k = \frac{1}{\langle \Psi_k^2 \rangle} \sum_{i=0}^{P} \sum_{j=0}^{P} \boldsymbol{u}^i \cdot \boldsymbol{v}^j \langle \Psi_i \Psi_j \Psi_k \rangle . \tag{6}$$

We denote this dot product in $(\mathcal{V}^p)^n$ by

$$\alpha = \boldsymbol{u} \odot \boldsymbol{v}.$$

Finally, we can consider random $n \times n$-matrices in $(\mathcal{V}^p)^{n \times n}$. Given $A \in (\mathcal{V}^p)^{n \times n}$ and $\boldsymbol{u} \in (\mathcal{V}^p)^n$ we denote the stochastic matrix-vector product in $\mathcal{V}^p$ of $A$ and $\boldsymbol{u}$ by $A \circledast \boldsymbol{u}$ with

$$(\mathcal{V}^p)^n \ni (A \circledast \boldsymbol{u}) = \sum_{k=0}^{P} (A \circledast \boldsymbol{u})^k \Psi_k, \qquad (A \circledast \boldsymbol{u})^k = \frac{1}{\langle \Psi_k^2 \rangle} \sum_{i=0}^{P} \sum_{j=0}^{P} A^i \boldsymbol{u}^j \langle \Psi_i \Psi_j \Psi_k \rangle .$$

*2.4. Uncertain dynamical systems*

Consider the deterministic autonomous ODE system,

$$\begin{cases} \dot{\boldsymbol{y}} = \boldsymbol{g}(\boldsymbol{y}), \\ \boldsymbol{y}(0) = \boldsymbol{y}_0, \end{cases} \tag{7}$$

where the solution of the system is a function $\boldsymbol{y} : [0, T_{fin}] \to \mathbb{R}^n$. We consider parametric uncertainty in the source term $\boldsymbol{g}$ and the initial conditions, i.e. $\boldsymbol{g} = \boldsymbol{g}(\boldsymbol{y}, \boldsymbol{\xi})$, and $\boldsymbol{y}_0 = \boldsymbol{y}_0(\boldsymbol{\xi})$. Thus, the solution of (7) is a

stochastic process,

$$\boldsymbol{y} : [0, T_{fin}] \times \Omega^* \to \mathbb{R}^n.$$

That is, one may view $\boldsymbol{y}$ as an indexed collection of random $n$-vectors, $\{\boldsymbol{y}(t)\}_{t\in[0,T_{fin}]}$, where for every $t \in [0, T_{fin}]$, $\boldsymbol{y}(t) : \Omega^* \to \mathbb{R}^n$ is a random $n$-vector. We can rewrite (7) more precisely as

$$\begin{cases} \dot{\boldsymbol{y}}(t, \boldsymbol{\xi}) = \boldsymbol{g}\big(\boldsymbol{y}(t, \boldsymbol{\xi}), \boldsymbol{\xi}\big) \\ \boldsymbol{y}(0, \boldsymbol{\xi}) = \boldsymbol{y}_0(\boldsymbol{\xi}). \end{cases} \qquad a.s. \tag{8}$$

For any given $\boldsymbol{\xi}$, the system has a deterministic trajectory $\{\boldsymbol{y}(t)\}_{t\in[0,T_{fin}]}$.

For the purpose of the discussion and subsequent developments, it will be useful to introduce the *nominal system*, which we define as a particular deterministic realization of the stochastic system in (8) corresponding to a given value $\boldsymbol{\xi} = \bar{\boldsymbol{\xi}} \in \Omega^*$. Although other choices for the nominal system may be relevant, we shall restrict ourselves to the selection $\bar{\boldsymbol{\xi}} = \langle \boldsymbol{\xi} \rangle$.

We shall assume that $\boldsymbol{y}(t, \boldsymbol{\xi}) \in L^2(\Omega^*)$ a.e. in $[0, T_{fin}]$ (component-wise), so $y_i(t, \boldsymbol{\xi})$ at a given time, can be approximated by a truncated PC expansion,

$$y_i(t, \boldsymbol{\xi}) = \sum_{k=0}^{P} y_i^k(t) \Psi_k(\boldsymbol{\xi}).$$

There are two classes of methods for computing the coefficients $y_i^k$ according to the definition of the projection used, namely the orthogonal projection onto $\mathcal{V}^p$ or the Galerkin projection. The orthogonal projection of $\boldsymbol{y}$ leads to the so-called non-intrusive methods which aim at computing the PC coefficients via a set of deterministic evaluations of $y(\boldsymbol{\xi})$ for specific realizations of $\boldsymbol{\xi}$; the Galerkin projection amounts to the resolution of an expanded system of ODEs resulting from the insertion of the PC expansion of $\boldsymbol{y}$ in the dynamical system (8) which is interpreted in a weak sense. In this paper, we primarily rely on the Galerkin projection, but will also rely on non-intrusive spectral projection [24] (NISP) in a limited fashion (see Sections 2.4.1 and 2.4.2 below for an overview of the NISP and the Galerkin method.)

*2.4.1. Non Intrusive Spectral Projection*

Let us focus on a generic component of the uncertain dynamical system (8) at a fixed time $t \in [0, T_{fin}]$ and simply denote this generic component by $y$. The NISP method defines the expansion coefficients $c_k$ in the expansion of $y(\boldsymbol{\xi})$ as the coordinates of its orthogonal projection on the space $\mathcal{V}^p$ spanned by the $\Psi_k$. The definition of orthogonal projection on $\mathcal{V}^p$ reads [35, 24, 2]:

$$\left( y - \sum_{l=0}^{P} c_l \Psi_l, \Psi_k \right) = 0, \quad k = 0, \ldots, P.$$

Therefore, by orthogonality of $\{\Psi_0, \ldots, \Psi_P\}$,

$$(y, \Psi_k) = \left( \sum_{l=0}^{P} c_l \Psi_l, \Psi_k \right) = \sum_{l=0}^{P} c_l \left( \Psi_l, \Psi_k \right) = c_k \left( \Psi_k, \Psi_k \right), \tag{9}$$

so the coefficient $c_k$ is given by

$$c_k = \frac{\langle y \Psi_k \rangle}{\langle \Psi_k^2 \rangle}. \tag{10}$$

In the case of Hermite or Legendre polynomials [1], the moments $\langle \Psi_k^2 \rangle$ in (10) can be computed analytically, and the determination of coefficients $c_k$ amounts tothe evaluation of the moments

$$\langle y \Psi_k \rangle = \int_{\Omega^*} y(\boldsymbol{s}) \Psi_k(\boldsymbol{s}) \, dF_{\boldsymbol{\xi}}(\boldsymbol{s}),$$

leading to the evaluation of $P+1$ integrals over $\Omega^* \subseteq \mathbb{R}^M$ to obtain each coefficient. The NISP method involves computation of the the above integrals via numerical integration. This can be done using a variety of methods, including random sampling Monte Carlo, or quasi-monte carlo, methods, as well as deterministic quadrature/sparse-quadrature methods [24]. In this work, owing to the low stochastic dimensionality of the problems considered, we rely on fully-tensorized Gauss quadrature for the evaluation of the integrals.

*2.4.2. The Galerkin method*

Consider the uncertain dynamical system (8). We seek to approximate $\boldsymbol{y}(t,\boldsymbol{\xi})$ by finding an expansion of $\boldsymbol{y}(t,\cdot)$ in $(\mathcal{V}^p)^n$ for $t \in [0, T_{fin}]$, $\boldsymbol{y}(t,\boldsymbol{\xi}) = \sum_{k=0}^{P} \boldsymbol{y}^k(t)\Psi_k(\boldsymbol{\xi})$, where $\boldsymbol{y}^k(t)$ are the stochastic modes of $\boldsymbol{y}(t)$. In components, we write

$$y_i(t,\boldsymbol{\xi}) = \sum_{k=0}^{P} y_i^k(t)\Psi_k(\boldsymbol{\xi}), \quad i = 1,\dots,n.$$

Inserting the truncated PC expansion of $\boldsymbol{y}$ in the ODE system (8) we obtain,

$$\begin{cases} \dfrac{d}{dt}\Big(\sum_{k=0}^{P} \boldsymbol{y}^k\Psi_k\Big) = \boldsymbol{g}\big(\sum_{k=0}^{P} \boldsymbol{y}^k\Psi_k, \boldsymbol{\xi}\big) + \boldsymbol{r}(t,\boldsymbol{\xi}), \\ \sum_{k=0}^{P} \boldsymbol{y}^k(0)\Psi_k = \boldsymbol{y}_0(\boldsymbol{\xi}) + \boldsymbol{r_0}(\boldsymbol{\xi}), \end{cases} \tag{11}$$

where $\boldsymbol{r}$ and $\boldsymbol{r_0}$ are the residuals arising from the truncation. Then, the modes $\boldsymbol{y}^k$ are defined such that the corresponding residuals are orthogonal to $\mathcal{V}^p$ [24], that is

$$\forall t \in [0, T_{fin}] \;\; (\boldsymbol{r}(t,\cdot), \Psi_k) = 0, \quad (\boldsymbol{r_0}, \Psi_k) = 0, \quad 0 \le k \le P.$$

This leads to the following system of equations

$$\begin{cases} \dot{\boldsymbol{y}}^k = \dfrac{1}{\langle\Psi_k^2\rangle}\left\langle \boldsymbol{g}\big(\sum_k \boldsymbol{y}^k\Psi_k, \boldsymbol{\xi}\big)\Psi_k \right\rangle \\ \boldsymbol{y}^k(t=0) = \dfrac{\langle \boldsymbol{y}_0(\cdot)\Psi_k\rangle}{\langle\Psi_k^2\rangle} \end{cases}, \quad k = 0,\dots,P. \tag{11'}$$

Setting $[\boldsymbol{y}] = (\boldsymbol{y}^0 \cdots \boldsymbol{y}^P)^T$, and similarly $[\tilde{\boldsymbol{g}}]$ for the stochastic modes of the right-hand-side, i.e.

$$\tilde{\boldsymbol{g}}^k([\boldsymbol{y}]) = \frac{\langle \boldsymbol{g}(\boldsymbol{y},\boldsymbol{\xi})\Psi_k\rangle}{\langle\Psi_k^2\rangle},$$

the dynamical equation can be recast as

$$[\dot{\boldsymbol{y}}] = [\tilde{\boldsymbol{g}}]([\boldsymbol{y}]),$$

showing that the Galerkin projection leads to the resolution of a set of $(P+1)\times n$ coupled deterministic ODEs.

*2.5. Some matrix theory concepts*

Here we collect some basics from matrix theory [23, 15, 30]. A matrix $S \in \mathbb{R}^{n\times n}$ is called $\mathbb{R}$-diagonalizable if it has real eigenvalues and a complete set of (real) eigenvectors; that is, the eigenvectors of $S$ form a basis of $\mathbb{R}^n$. Usually, when talking about eigenvectors of $S$ without no qualifications, we refer to the right eigenvectors. In the current work, the left eigenvectors are of importance also; recall that a vector $\boldsymbol{b} \in \mathbb{R}^n$ is a left eigenvector corresponding to an eigenvalue $\lambda$ of $S$ if $\boldsymbol{b}^T S = \lambda \boldsymbol{b}^T$.

In particular, we are interested in real $n \times n$ matrices with $n$-distinct real eigenvalues. Such matrices are automatically $\mathbb{R}$-diagonalizable. Let $S$ be such a matrix, with distinct real eigenvalues $\{\lambda_1, \ldots, \lambda_n\}$ and right and left eigenvectors, $\{\boldsymbol{a}_1, \ldots, \boldsymbol{a}_n\}$ and $\{\boldsymbol{b}_1, \ldots, \boldsymbol{b}_n\}$. Note that

$$\lambda_j \boldsymbol{b}_j^T \boldsymbol{a}_i = \boldsymbol{b}_j^T S \boldsymbol{a}_i = \boldsymbol{b}_j^T (\lambda_i \boldsymbol{a}_i) = \lambda_i \boldsymbol{b}_j^T \boldsymbol{a}_i,$$

so that $(\lambda_i - \lambda_j)\boldsymbol{b}_j^T \boldsymbol{a}_i = 0$. Hence, $\boldsymbol{b}_j^T \boldsymbol{a}_i = 0$ for $i \neq j$. The left eigenvectors are usually normalized so that $\boldsymbol{b}_j^T \boldsymbol{a}_i = \delta_{ij}$. We refer to the basis formed by the left eigenvectors as the dual basis of that formed by the right eigenvectors. The right eigenvectors $\boldsymbol{a}_i$ of $S$ form a basis for $\mathbb{R}^n$ (as well as the left eigenvectors $\boldsymbol{b}_i$), and thus given any $\boldsymbol{x} \in \mathbb{R}^n$, we have

$$\boldsymbol{x} = \sum_{i=1}^{n} f_i \boldsymbol{a}_i. \tag{12}$$

We can compute the coefficients $f_i$ via the dual basis through $f_i = \boldsymbol{b}_i^T \boldsymbol{x}$. This decomposition is central in the CSP method for reduction of an ODE system, where we use the respective eigenvector bases of the system Jacobian, and decompose the right-hand-side of the system. In the CSP context, the coefficients $f_i$ in (12) are referred to as the mode amplitudes.

### *2.6. Overview of deterministic CSP*

In this section, we briefly outline the essential elements of Computational Singular Perturbation (CSP), particularly as used to tackle stiffness in (deterministic) chemical systems. As discussed in [19, 21, 40, 42], the CSP integrator addresses stiffness of the system by projecting out the fast time scales from the detailed chemical source term. This enables the use of explicit time integrators with large time steps, resulting in computational speedup.

Consider a deterministic ODE system such as the one in (7). The time scales $\{\tau_i\}_1^n$ of the system are defined as the magnitudes of the reciprocals of the eigenvalues for the Jacobian matrix $J = \nabla \boldsymbol{g} \in \mathbb{R}^{n \times n}$, $\tau_i = \frac{1}{|\lambda_i|}$; we assume that there are $n$-distinct timescales ordered as follows:

$$\tau_1 < \tau_2 < \cdots < \tau_n.$$

Note that this implies that $J$ has $n$ distinct eigenvalues, we further assume that the eigenvalues of $J$ are real.

In the CSP context, we may write the system in (7) as follows:

$$\dot{\boldsymbol{y}} = \boldsymbol{g}(\boldsymbol{y}) = \sum_{i=1}^{n} \boldsymbol{a}_i f_i, \tag{13}$$

where, following [42], we let the CSP vectors $\boldsymbol{a}_i$ and co-vectors $\boldsymbol{b}_i$ to be the right and left eigenvectors of $J$ respectively. As noted, we have $f_i = \boldsymbol{b}_i^T \boldsymbol{g}$. The coefficient $f_i$ represents the amplitude of mode $i$ and as $\boldsymbol{a}_i f_i$ becomes negligible, in the sense made precise below, the $i^{th}$ mode is classified as "fast". In the CSP parlance, a fast mode is "exhausted" if its amplitude is small as a result of near-equilibration of opposed non-negligible processes, while it is "frozen" if it is composed of essentially negligible processes. The distinction is obviously problem-specific, but both classes are generally referred to as fast modes. Suppose the first $m$ modes are fast; then, we have,

$$\dot{\boldsymbol{y}} = \underbrace{\sum_{i=1}^{m} \boldsymbol{a}_i f_i}_{\boldsymbol{g}_{\text{fast}} \approx 0} + \underbrace{\sum_{i=m+1}^{n} \boldsymbol{a}_i f_i}_{\boldsymbol{g}_{\text{slow}}} \approx \sum_{i=m+1}^{n} \boldsymbol{a}_i f_i = \underbrace{(I - \sum_{i=1}^{m} \boldsymbol{a}_i \boldsymbol{b}_i^T)}_{P} \boldsymbol{g} =: P\boldsymbol{g}.$$

The "slow" equation $\dot{\boldsymbol{y}} = P\boldsymbol{g}(\boldsymbol{y})$ is then simple to integrate, because it involves timescales greater than or

equal to $\tau_{m+1}$. We deem the $m^{th}$ time process fast [40] when the following vectorial inequality is met:

$$\tau_{m+1} \times |\sum_{i=1}^{m} \boldsymbol{a}_i f_i| < \varepsilon_{rel}|\boldsymbol{y}| + \varepsilon_{abs}\mathbf{1}. \tag{14}$$

Here $|\boldsymbol{y}|$ denotes the vector whose elements are absolute values of the entries of the $n$-dimensional vector $\boldsymbol{y}$, $\mathbf{1}$ is the vector of ones $\mathbf{1} = (1, 1, \ldots, 1)^T \in \mathbb{R}^n$, and $\varepsilon_{rel}$ and $\varepsilon_{abs}$ are user specified tolerances. The simplified non-stiff ODE system $\dot{\boldsymbol{y}} = P\boldsymbol{g}(\boldsymbol{y})$ can then be integrated using time steps on the order of $\alpha\tau_{m+1}$ with $0 < \alpha \lesssim 1$ [40, 44]. We outline one-step of the CSP integrator in Algorithm 1.

**Algorithm 1** One step of the CSP time integrator (assuming modes $1, \ldots, m$ are fast)

$\Lambda(t) = \left[\Lambda_{ij}(t)\right] = \left(\dot{\boldsymbol{b}}_i^T + \boldsymbol{b}_i^T J\right)\boldsymbol{a}_j\Big|_t$

$\Gamma(t) = \left(\Lambda(t)\right)^{-1}$

$\hat{\boldsymbol{y}}(t+\Delta t) = \boldsymbol{y}(t) + \int_t^{t+\Delta t} P\boldsymbol{g}(\boldsymbol{y}(s))\, ds$ {Integration of the slow dynamics}

$f_j(t) = \boldsymbol{b}_i(t) \cdot \boldsymbol{g}\left[\hat{\boldsymbol{y}}(t+\Delta t)\right], \quad j = 1, \ldots, m$

$\delta\boldsymbol{y}(t) = \sum_{i=1}^{m} \gamma_i(t)\boldsymbol{a}_i(t), \quad$ where $\gamma_i(t) = \sum_{j=1}^{m} \Gamma_{ij}(t) f_j(t)$

$\boldsymbol{y}(t+\Delta t) = \hat{\boldsymbol{y}}(t+\Delta t) - \delta\boldsymbol{y}(t)$ {Radical correction}

**Remark 1.** *Initially, with $m = 0$, the full ODE system (8) is integrated with no CSP simplification and using time steps on the order of $\alpha\tau_1$ with $0 < \alpha \lesssim 1$.*

**Remark 2.** *In the present implementation of CSP, we use the approximation:*

$$\int_t^{t+\Delta t} P\boldsymbol{g}(\boldsymbol{y}(s))\, ds \approx \Delta t \times P\boldsymbol{g}(\boldsymbol{y}(t)),$$

*which amounts to using the (reduced) Euler's method:*

$$\boldsymbol{y}(t+\Delta t) = \boldsymbol{y}(t) + \Delta t \times P\boldsymbol{g}(\boldsymbol{y}(t)) - \delta\boldsymbol{y}(t).$$

## 3. Stochastic system Jacobian

Consider the uncertain dynamical system (8). For each $\boldsymbol{\xi} \in \Omega^*$, we have a corresponding system trajectory and also a system Jacobian, $J(\boldsymbol{\xi})$,

$$J_{ij} = \frac{\partial g_i}{\partial y_j}, \quad i, j = 1, \ldots, n. \tag{15}$$

We shall further assume that the stochastic Jacobian $J$ is in $\left(L^2(\Omega^*)\right)^{n\times n}$ and is almost surely $\mathbb{R}$-diagonalizable with $n$ distinct (stochastic) eigenvalues. In the scope of the present simplified CSP reduction approach, we are interested in defining a spectral representation of $J(\boldsymbol{\xi})$ according to:

$$J(\boldsymbol{\xi}) = \sum_{k=0}^{P} J^k \Psi_k(\boldsymbol{\xi}), \quad \boldsymbol{\xi} \in \Omega^*. \tag{16}$$

Interest in such a spectral representation of $J$ stems from two main reasons. In the first place, we would like to characterize the dependence of system eigenvectors on the uncertainty given by $\boldsymbol{\xi}$. Secondly, we would like to explore the CSP reduction using *nominal eigenvectors*, i.e. the eigenvectors of the nominal system.

Therefore, it is necessary to have an expression of the Jacobian that preserves the physical interpretation of its eigenvectors; that is, each eigenvector is in $\mathbb{R}^n$.

Consider the Galerkin system (11′). We denote the corresponding Jacobian by $\mathcal{J}$ which is a (deterministic) $N \times N$ matrix with $N = n(P+1)$. Let $\boldsymbol{u}$ be a random $n$-vector in $\mathcal{V}^p$ with spectral expansion $\boldsymbol{u} = \sum_{k=0}^{P} \boldsymbol{u}^k \Psi_k$. As mentioned in Section 2.3, the modes $\boldsymbol{u}^k$ define the coordinates of $\boldsymbol{u}$ in $(\mathcal{V}^p)^n$ which we denote by $[\boldsymbol{u}]$. The matrix $\mathcal{J} \in \mathbb{R}^{N\times N}$ is indexed [24, 9] so that it acts on a random $n$-vector $\boldsymbol{u} \in (\mathcal{V}^p)^n$ through its coordinate vector $[\boldsymbol{u}]$ as follows:

$$\mathcal{J}[\boldsymbol{u}] = \begin{pmatrix} \mathcal{J}^{00} & \mathcal{J}^{01} & \dots & \mathcal{J}^{0P} \\ \mathcal{J}^{10} & \mathcal{J}^{11} & \dots & \mathcal{J}^{1P} \\ & \cdots\cdots\cdots & & \\ \mathcal{J}^{P0} & \mathcal{J}^{P1} & \dots & \mathcal{J}^{PP} \end{pmatrix} \begin{pmatrix} \boldsymbol{u}^0 \\ \boldsymbol{u}^1 \\ \vdots \\ \boldsymbol{u}^P \end{pmatrix},$$

with $\mathcal{J}^{kl} \in \mathbb{R}^{n\times n}$ defined by [36]

$$\left\langle \Psi_k^2 \right\rangle \mathcal{J}_{ij}^{kl} = \left\langle J_{ij}(\boldsymbol{y}) \Psi_k \Psi_l \right\rangle, \quad i,j = 1,\dots,n,\ k,l = 0,\dots,P. \tag{17}$$

### *3.1. Relationship between $\mathcal{J}$ and $J$*

Here we derive a simple relationship between the spectral representations for $J$ in (16) and the matrix $\mathcal{J} = \left(\mathcal{J}_{ij}^{kl}\right)$ defined in (17). For $i,j = 1,\dots,n$ and $k = 0,\dots,P$ we have

$$\mathcal{J}_{ij}^{k0} = \frac{\langle J_{ij}\Psi_k\Psi_0\rangle}{\langle \Psi_k^2\rangle} = \frac{\left\langle (\sum_{m=0}^{P} J_{ij}^m \Psi_m)\Psi_k \right\rangle}{\langle \Psi_k^2\rangle} = \sum_{m=0}^{P} J_{ij}^m \frac{\langle \Psi_k\Psi_m\rangle}{\langle \Psi_k^2\rangle} = \sum_{m=0}^{P} J_{ij}^m \frac{\delta_{km}\left\langle \Psi_m^2\right\rangle}{\langle \Psi_k^2\rangle} = J_{ij}^k.$$

That is,

$$\mathcal{J}^{k0} = J^k, \quad k = 0,\dots,P. \tag{18}$$

### *3.2. The affine case*

In the example below, we will consider the situation where the Jacobian $J$ is an affine function of the system variables (see Section 5.1). In this case $J$ is given by

$$J_{ij}(\boldsymbol{y}) = \sum_{m=1}^{n} a_{ij}^m y_m + b_{ij}, \quad i,j = 1,\dots,n. \tag{19}$$

Inserting (19) into (17) and using the PC expansion of $y_m$ leads to:

$$\mathcal{J}_{ij}^{kl} = \sum_{m=1}^{n}\sum_{s=0}^{P} y_m^s \frac{\left\langle a_{ij}^m \Psi_s\Psi_k\Psi_l\right\rangle}{\langle \Psi_k^2\rangle} + \frac{\langle b_{ij}\Psi_k\Psi_l\rangle}{\langle \Psi_k^2\rangle}. \tag{20}$$

In the case where $a_{ij}^m$ and $b_{ij}$ are deterministic (20) simplifies to

$$\mathcal{J}_{ij}^{kl} = \sum_{m=1}^{n} a_{ij}^m \sum_{s=0}^{P} y_m^s \frac{\langle \Psi_s\Psi_k\Psi_l\rangle}{\langle \Psi_k^2\rangle} + b_{ij}\delta_{kl}. \tag{21}$$

In Section 5.1, we will consider $a_{ij}^m$ and $b_{ij}$ that are uniformly distributed random variables of form

$$a_{ij}^m = \bar{\alpha}_{ij}^m + \alpha_{ij}^m \xi_1, \qquad b_{ij} = \bar{\beta}_{ij} + \beta_{ij}\xi_2, \qquad \xi_1,\xi_2 \overset{iid}{\sim} \mathcal{U}(-1,1),$$

where $\bar{\alpha}_{ij}^m$, $\alpha_{ij}^m$, $\bar{\beta}_{ij}$, and $\beta_{ij}$ are constants. Inserting the expressions for $a_{ij}^m$ and $b_{ij}$ in (20) gives:

$$\mathcal{J}_{ij}^{kl} = \sum_{m=1}^{n} \bar{\alpha}_{ij}^m \sum_{s=0}^{P} y_m^s \frac{\langle \Psi_s \Psi_k \Psi_l \rangle}{\langle \Psi_k^2 \rangle} + \sum_{m=1}^{n} \alpha_{ij}^m \sum_{s=0}^{P} y_m^s \frac{\langle \xi \Psi_s \Psi_k \Psi_l \rangle}{\langle \Psi_k^2 \rangle} + \bar{\beta}_{ij} \delta_{kl} + \beta_{ij} \frac{\langle \xi \Psi_k \Psi_l \rangle}{\langle \Psi_k^2 \rangle}.$$

*3.3. Solving the stochastic eigenvalue problem*

Here we discuss computation of the chaos coefficients of the eigenvalues $\lambda(\boldsymbol{\xi})$ and right eigenvectors $\boldsymbol{a}(\boldsymbol{\xi})$ of the stochastic Jacobian by solving the following eigenvalue problem:

$$J(\boldsymbol{\xi})\boldsymbol{a}(\boldsymbol{\xi}) = \lambda(\boldsymbol{\xi})\boldsymbol{a}(\boldsymbol{\xi}), \qquad \boldsymbol{a}(\boldsymbol{\xi}) \cdot \boldsymbol{a}(\boldsymbol{\xi}) = 1, \tag{22}$$

where $\cdot$ denotes the Euclidean inner product in $\mathbb{R}^n$. The PC representations of $\lambda(\boldsymbol{\xi})$ and $\boldsymbol{a}(\boldsymbol{\xi})$ are

$$\lambda(\boldsymbol{\xi}) = \sum_{k=0}^{P} \lambda^k \Psi_k, \qquad \boldsymbol{a}(\boldsymbol{\xi}) = \sum_{k=0}^{P} \boldsymbol{a}^k \Psi_k. \tag{23}$$

Using (18) to recover the PC representation of $J(\boldsymbol{\xi})$,

$$J(\boldsymbol{\xi}) = \sum_{k=0}^{P} J^k \Psi_k(\boldsymbol{\xi}), \quad J^k = \mathcal{J}^{k0},$$

and using the PC representations of $\lambda$, $\boldsymbol{a}$, and $J$ in conjunction with (22), we obtain

$$\sum_{i=0}^{P}\sum_{j=0}^{P} \left(J^i - \lambda^i I\right) \boldsymbol{a}^j \Psi_i \Psi_j = r_1, \qquad \sum_{i=0}^{P}\sum_{j=0}^{P} \boldsymbol{a}^i \cdot \boldsymbol{a}^j \Psi_i \Psi_j - 1 = r_2, \tag{24}$$

where $I$ is the $n \times n$ identity matrix, and $r_1$ and $r_2$ are the residuals due to the finite truncation of the PC expansions. Following the method of Ghanem and Ghosh [9], these residuals are minimized by forcing their orthogonality to the basis of $\mathcal{V}^p$. The stochastic eigenvalue problem becomes:

$$\begin{cases} \displaystyle\sum_{i=0}^{P}\sum_{j=0}^{P} \left(J^i - \lambda^i I\right) \boldsymbol{a}^j \langle \Psi_i \Psi_j \Psi_k \rangle = 0, \quad k = 0, \ldots, P, \\ \displaystyle\sum_{i=0}^{P}\sum_{j=0}^{P} \boldsymbol{a}^i \cdot \boldsymbol{a}^j \langle \Psi_i \Psi_j \Psi_k \rangle - \delta_{k0} = 0, \quad k = 0, \ldots, P. \end{cases} \tag{25}$$

Note that using the notation of Section 2.3 the system (25) can be simply expressed as:

$$\begin{cases} (J - \lambda I) \circledast \boldsymbol{a} = \boldsymbol{0}, \\ \boldsymbol{a} \odot \boldsymbol{a} = 1. \end{cases}$$

We compute $\lambda_k$ and $\boldsymbol{a}^k$ for $k = 0 \ldots P$ by solving the nonlinear system in (25) using Newton-Raphson iterations, and refer to this approach as the residual minimization method.

**Remark 3.** *The method of Ghanem and Ghosh [9] is formulated to compute the right stochastic eigenvectors. In our current study, we need to compute the left stochastic eigenvectors as well. That is, we need to solve the following problem:*

$$\boldsymbol{b}(\boldsymbol{\xi})^T J(\boldsymbol{\xi}) = \lambda(\boldsymbol{\xi})\boldsymbol{b}(\boldsymbol{\xi})^T, \qquad \boldsymbol{b}(\boldsymbol{\xi}) \cdot \boldsymbol{b}(\boldsymbol{\xi}) = 1.$$

*This can be performed easily by the same method as above except we replace $J^i$ by $(J^i)^T$ in (25).*

*3.4. Relation between nominal and stochastic eigenvectors*

Consider the eigenpairs of the nominal system Jacobian $\bar{J} = J(\bar{\boldsymbol{\xi}})$,

$$(\bar{\lambda}_i, \bar{\boldsymbol{a}}_i), \quad \bar{\boldsymbol{a}}_i \cdot \bar{\boldsymbol{a}}_i = 1, \quad i = 1, \ldots, n,$$

where we have used overbars to indicate that these eigenpairs correspond to the nominal system Jacobian. Here we work under the assumption that each $\bar{\lambda}_i$ is real and *simple*, i.e. with multiplicity one. For a given $\boldsymbol{\xi} \in \Omega^*$, consider the eigenpair $(\lambda_i(\boldsymbol{\xi}), \boldsymbol{a}_i(\boldsymbol{\xi}))$ of $J(\boldsymbol{\xi})$, where $\boldsymbol{a}_i$ is a *unit* eigenvector. Under the assumption that $\lambda_i(\boldsymbol{\xi})$ is a simple eigenvalue, the choice of $\boldsymbol{a}_i(\boldsymbol{\xi})$ is unique up to its sign. To make the choice of $\boldsymbol{a}_i$ unique, we may multiply $\boldsymbol{a}_i$ by $\operatorname{sgn}(\boldsymbol{a}_i \cdot \bar{\boldsymbol{a}}_i)$, where sgn denotes the signum function.

Assuming that $J$ depends continuously on the parameter $\boldsymbol{\xi}$, it is well known [23] that the eigenvalues of $J(\boldsymbol{\xi})$ depend continuously on $\boldsymbol{\xi}$; that is, for each eigenvalue $\lambda_i(\boldsymbol{\xi})$, we have $\lim_{\boldsymbol{\xi} \to \bar{\boldsymbol{\xi}}} \lambda_i(\boldsymbol{\xi}) = \bar{\lambda}_i$. In the case $J$ depends differentiably on $\boldsymbol{\xi}$, we can say that an eigenvector of $J(\boldsymbol{\xi})$ (chosen as above to make it unique for each $\boldsymbol{\xi}$) corresponding to a simple eigenvalue depends differentiably on $\boldsymbol{\xi}$ in a neighborhood of $\boldsymbol{\xi} = \bar{\boldsymbol{\xi}}$ (see for example [23, Theorem 8, P. 102]); this in particular implies that,

$$\lim_{\boldsymbol{\xi} \to \bar{\boldsymbol{\xi}}} \boldsymbol{a}_i(\boldsymbol{\xi}) = \boldsymbol{a}_i(\bar{\boldsymbol{\xi}}) = \bar{\boldsymbol{a}}_i. \tag{26}$$

A measure of deviation of $\boldsymbol{a}_i(\boldsymbol{\xi})$ from $\bar{\boldsymbol{a}}$ is the angle $\zeta_i$ bewteen them:

$$\cos(\zeta_i(\boldsymbol{\xi})) = \boldsymbol{a}_i(\boldsymbol{\xi}) \cdot \bar{\boldsymbol{a}}_i. \tag{27}$$

Moreover, by the assumptions on the eigen-structure of the the nominal system Jacobian, the eigenvectors $\bar{\boldsymbol{a}}_i$ form a basis of $\mathbb{R}^n$. Therefore, we may expand the vectors $\boldsymbol{a}_i$ in the basis $\{\bar{\boldsymbol{a}}_1, \ldots, \bar{\boldsymbol{a}}_n\}$:

$$\boldsymbol{a}_i(\boldsymbol{\xi}) = \sum_{j=1}^{n} h_{ij}(\boldsymbol{\xi}) \bar{\boldsymbol{a}}_i. \tag{28}$$

The coefficients $h_{ij}$ provide a further means to assess how close the eigenvectors are to those of the nominal system. Note that,

$$\bar{\boldsymbol{b}}_k \cdot \boldsymbol{a}_i(\boldsymbol{\xi}) = \bar{\boldsymbol{b}}_k \cdot \Big( \sum_{j=1}^{n} h_{ij}(\boldsymbol{\xi}) \bar{\boldsymbol{a}}_i \Big) = h_{ik}(\boldsymbol{\xi}).$$

That is, $h_{ij}(\boldsymbol{\xi}) = \bar{\boldsymbol{b}}_j \cdot \boldsymbol{a}_i(\boldsymbol{\xi})$. We find it convenient to consider the matrix $H = H(\boldsymbol{\xi})$ defined by $H_{ij} = h_{ij}$, $i, j = 1, \ldots, n$.

In view of (26) we have

$$\lim_{\boldsymbol{\xi} \to \bar{\boldsymbol{\xi}}} \cos(\zeta_i(\boldsymbol{\xi})) = 1, \tag{29}$$

and

$$\lim_{\boldsymbol{\xi} \to \bar{\boldsymbol{\xi}}} h_{ij}(\boldsymbol{\xi}) = \lim_{\boldsymbol{\xi} \to \bar{\boldsymbol{\xi}}} \bar{\boldsymbol{b}}_j \cdot \boldsymbol{a}_i(\boldsymbol{\xi}) = \bar{\boldsymbol{b}}_j \cdot \bar{\boldsymbol{a}}_i = \delta_{ij}.$$

That is, $\lim_{\boldsymbol{\xi} \to \bar{\boldsymbol{\xi}}} h_{ij} = \delta_{ij}$; this can be written more concisely as

$$\lim_{\boldsymbol{\xi} \to \bar{\boldsymbol{\xi}}} \|H(\boldsymbol{\xi}) - I\|_F = 0, \tag{30}$$

where $\|\cdot\|_F$ denotes the Frobenius norm:

$$\|A\|_F = \Big( \sum_{i=1}^{m} \sum_{j=1}^{n} |A_{ij}|^2 \Big)^{1/2}, \quad A \in \mathbb{R}^{m \times n}.$$

In the computations below, we shall use the uncertainty measures $\cos(\zeta_i(\boldsymbol{\xi}))$ and

$$\eta(\boldsymbol{\xi}) = \|H(\boldsymbol{\xi}) - I\|_F$$

to study the deviation of the stochastic eigenvectors from their nominal counterparts.

## 4. The simplified CSP framework

In this section, we generalize the CSP method introduced in Section 2.6 to the stochastic case. Following the analysis above, our approach is based on exploiting the spectral representation of the $n$-dimensional stochastic eigenvectors as CSP vectors. Accordingly, the resulting CSP formalism involves a projection onto a stochastic manifold. Below, we develop two variants of the present simplified stochastic CSP methodology. The first, outlined in Section 4.1, is based on using the stochastic eigenvectors as CSP vectors. The second variant, outlined in Section 4.2, is based on using the deterministic eigenvectors of the nominal system as CSP vectors. The latter is inspired by the observation that for the present system, whereas the stochastic eigenvalues exhibit a pronounced dependence on $\boldsymbol{\xi}$, the stochastic eigenvectors are weakly sensitive to the uncertainty; thus, in this case, the simplified CSP algorithm involves projection onto a deterministic manifold, though the projection still involves stochastic mode amplitudes. As further discussed in Section 6, this can lead to substantial computational savings. One of the main advantages offered by both of these methods is enabling a natural extension of the deterministic CSP algorithm (cf. Section 2.6) to the stochastic case by providing simplified (averaged) criteria for determination of (stochastic) fast subspaces of an uncertain ODE system.

### *4.1. Stochastic eigenvectors as CSP vectors*

For the uncertain system (8), we seek a decomposition of the system right-hand-side as in (13), namely in terms of the stochastic eigenvectors of $J(\boldsymbol{\xi})$. By our assumptions on the eigen-structure of $J(\boldsymbol{\xi})$, we know that its right eigenvectors $\{\boldsymbol{a}_1, \ldots, \boldsymbol{a}_n\}$ form a basis of $\mathbb{R}^n$ and hence $\boldsymbol{g}$ can be expanded in this basis; however, the expansion coefficients $f_i$ will also be random. Considering the weak form of (13), we arrive at:

$$\dot{\boldsymbol{y}} = \boldsymbol{g}(\boldsymbol{y}) \approx \sum_{i=1}^{n} \boldsymbol{a}_i \circledast f_i, \tag{31}$$

with $\boldsymbol{y} \in (\mathcal{V}^p)^n$, $\boldsymbol{a}_i \in (\mathcal{V}^p)^n$, and $f_i \in \mathcal{V}^p$. Thus, we have to compute the $n$ stochastic coordinates $f_i(\boldsymbol{\xi})$ of the system right-hand side in the space spanned by the right stochastic eigenvectors. The coefficients $f_i$ are evaluated using the Galerkin dot product:

$$f_i \approx \boldsymbol{b}_i \odot \boldsymbol{g}, \tag{32}$$

where we have relied on the approximate orthogonality between the stochastic left and right eigenvectors.

With $m$ fast modes, the system (31) is reduced according to:

$$\dot{\boldsymbol{y}} \approx \sum_{i=m+1}^{n} \boldsymbol{a}_i \circledast f_i \approx \underbrace{(I - \sum_{i=1}^{m} \boldsymbol{a}_i \circledast \boldsymbol{b}_i)}_{P} \circledast \boldsymbol{g} =: P \circledast \boldsymbol{g}. \tag{33}$$

The difficulty in the stochastic case is that in general $m$ will depend on $\boldsymbol{\xi}$. Instead of seeking a criterion guaranteeing $m$ fast modes for all (or almost all) $\boldsymbol{\xi} \in \Omega^*$, which is a difficult task, we formulate an approximate criterion in a mean-square sense. Specifically, we deem the first $m$ modes fast if the following inequality holds:

$$\left\langle (\tau_{m+1} \circledast \sum_{i=1}^{m} \boldsymbol{a}_i \circledast f_i)^2 \right\rangle < \varepsilon_{rel} \left\langle \boldsymbol{y}^2 \right\rangle + \varepsilon_{abs} \mathbf{1}, \tag{34}$$

where it is understood that the square operator applies component-wise on the corresponding vectors [41]; that is, $\boldsymbol{y}^2$ denotes a vector whose $n$ components are the squares of the corresponding components of $\boldsymbol{y}$. Note that the criterion in (34) is convenient to implement, because in actual computations the stochastic quantities are represented by their coordinates in the orthogonal basis of $\mathcal{V}^p$. For instance,

$$\left\langle \boldsymbol{y}^2 \right\rangle = \sum_{k=0}^{P} \left\langle \Psi_k^2 \right\rangle \left(\boldsymbol{y}^k\right)^2.$$

Different criteria can be considered also, as further discussed in Section 4.1.2.

*4.1.1. Algorithm for simplified CSP with stochastic eigenvectors*

Assembling all the previous components, we end up with the following stochastic CSP algorithm 2, for the integration of the solution over a time step. Note that for a system with $m$ fast modes, Algorithm 2 can be used for integration of the simplified stochastic system $\dot{\boldsymbol{y}} = P \circledast \boldsymbol{g}$ with time steps on the order of $\alpha\tau_{m+1}^0$ with $0 < \alpha \lesssim 1$. Note that $\tau_{m+1}^0$ is the mean of $\tau_{m+1}$.

**Algorithm 2** One step of CSP integration (assuming modes $1, \ldots, m$ are fast) for the stochastic system using the stochastic right eigenvectors as CSP vectors.

$\Lambda(t) = \left[\Lambda_{ij}(t)\right] = \left(\dot{\boldsymbol{b}}_i^T + \boldsymbol{b}_i^T \circledast J\right) \circledast \boldsymbol{a}_j\Big|_t$

$\Gamma(t) = \left(\Lambda(t)\right)^{-1}$

$\hat{\boldsymbol{y}}(t+\Delta t) = \boldsymbol{y}(t) + \int_t^{t+\Delta t} P \circledast \boldsymbol{g}(\boldsymbol{y}(s))\, ds$ {Integration of the slow dynamics}

$f_j(t) = \boldsymbol{b}^j(t) \odot \boldsymbol{g}\left[\hat{\boldsymbol{y}}(t+\Delta t)\right], \quad j = 1, \ldots, m$

$\delta\boldsymbol{y}(t) = \sum_{i=1}^{m} \gamma_i(t) \circledast \boldsymbol{a}_i(t), \quad$ where $\gamma_i(t) = \sum_{j=1}^{m} \Gamma_{ij}(t) \circledast f_j(t)$

$\boldsymbol{y}(t+\Delta t) = \hat{\boldsymbol{y}}(t+\Delta t) - \delta\boldsymbol{y}(t)$ {Radical correction}

We observe that Algorithm 2 involves solving the stochastic eigenproblem along with several Galerkin products. In addition, it involves the inversion of the stochastic matrix $\Lambda(t)$, which can be accomplished either through a Galerkin linear solve as outlined in [24] or adaptation of an iterative method for approximation of a matrix inverse to the stochastic case as outlined in Appendix A. In cases when the nominal system dynamics can be reliably used to approximate the stochastic system trajectory, we may use the nominal system eigenvectors as CSP vectors as discussed in Section 4.2; we will see that using the basis of eigenvectors of the nominal system Jacobian simplifies many of the computational steps in Algorithm 2.

*4.1.2. Remarks*

The criterion (34) was derived by mimicking its deterministic counterpart. We note that by using such averaged criteria we are paying two penalties. In particular, at any time step where we deem $m$ modes fast, some realizations may not satisfy the corresponding deterministic criterion. Conversely, there will be realizations which would have been deemed fast at an earlier time, but are still retained in the simplified interpretation above. Thus, generally, the simplified interpretation in (34) may lead to higher projection errors than one would anticipated based on the specified threshold, and also to a suboptimal integration efficiency. On the other hand, the advantage of the present approach is that it naturally leads to a characterization of the fast and slow manifolds in $\mathbb{R}^n$ due to the uncertainty germ $\boldsymbol{\xi}$.

Also, note that alternate strategies are possible for picking a criterion based on definition of *global* characteristic timescales. An example illustrating this alternative is provided, based on the observation that the stochastic eigenvalues yield information on the timescales for every $\boldsymbol{\xi} \in \Omega^*$. In particular, if the timescales $\tau_i \in \mathbb{R}^+$ associated to each stochastic eigenvector $\boldsymbol{a}_i$ can be suitably bounded, one can then exploit the appropriate bound to determine a unique number $m$ of fast modes that is valid over the whole

uncertainty range. An approximation for the global timescale may be based on the second moment of the associated eigenvalue:

$$\bar{\bar{\tau}}_i = \frac{1}{\sqrt{\langle \lambda_i^2 \rangle}}. \tag{35}$$

Similarly, the deterministic criterion (14) can be extended in the stochastic case by replacing the absolute values by $L^2$-norms. This results in the alternate criterion

$$\bar{\bar{\tau}}_{m+1} \times \left\langle \Big( \sum_{i=1}^{m} \boldsymbol{a}_i \circledast f_i \Big)^2 \right\rangle^{1/2} < \epsilon_{ref} \left\langle \big(\boldsymbol{y}\big)^2 \right\rangle^{1/2} + \varepsilon_{abs} \mathbf{1}, \tag{36}$$

where as before it is understood that the square and square root operators apply component-wise on vectors. For a system with $m$ fast modes, Algorithm 2 can be used for integration of the simplified stochastic system $\dot{\boldsymbol{y}} = P \circledast \boldsymbol{g}$, with time steps of the order of $\alpha \bar{\bar{\tau}}_{m+1}$ with $0 < \alpha \lesssim 1$. Note that owing to the definition of a global characterization of the timescales, as opposed to (34), one avoids the need to compute the PC expansion of $(\lambda_i(\boldsymbol{\xi}))^{-1}$.

### *4.2. Nominal system eigenvectors as CSP vectors*

We have seen that the extension of the deterministic CSP method to the stochastic case involves the calculation of the left and right stochastic eigenvectors and eigenvalues of the stochastic Jacobian $J(\boldsymbol{\xi})$. These are computed through the solution of nonlinear deterministic problems after stochastic discretization in $\mathcal{V}^p$. It can be anticipated that the determination of the stochastic eigenspaces constitutes the most computationally demanding part of the stochastic CSP method, justifying the question of the possibility to bypass this step in order to reduce the computational cost. In many cases, as it will be shown later for the example treated in the paper, the uncertainty in the system induces a moderate variability of the eigenvectors, such that the stochastic eigenvectors can be well approximated by the deterministic eigenvectors of the nominal Jacobian $\bar{J} = J(\bar{\boldsymbol{\xi}})$, allowing for the expansion of the stochastic system right-hand-side in the basis of the deterministic nominal eigenvectors. Using the nominal system eigenvectors for CSP vectors effectively uses the dynamics of the nominal system as a guide for determining the fast and slow subspaces for the uncertain system. This approach involves significant computational savings highlighted by not having to compute the stochastic eigenvectors.

Assuming such approximation is valid, we begin by reformulating the uncertain system (8) by expanding its right-hand-side in the basis of the nominal eigenvectors $\{\bar{\boldsymbol{a}}_1, \ldots, \bar{\boldsymbol{a}}_n\}$:

$$\dot{\boldsymbol{y}} = \boldsymbol{g}(\boldsymbol{y}) = \sum_{i=1}^{n} \bar{\boldsymbol{a}}_i f_i. \tag{37}$$

The expansion coefficients (mode amplitudes) $f_i$ are stochastic and are given by

$$f_i(\boldsymbol{\xi}) = \bar{\boldsymbol{b}}_i^T \boldsymbol{g}(\boldsymbol{y}, \boldsymbol{\xi}), \quad i = 1, \ldots, n, \tag{38}$$

where $\bar{\boldsymbol{b}}_{\boldsymbol{i}} \in \mathbb{R}^n$ are the nominal left eigenvectors.

The stochastic equation (37) can be projected onto $\mathcal{V}^p$, resulting in

$$\dot{\boldsymbol{y}}^k = \sum_{i=1}^{n} \bar{\boldsymbol{a}}_i f_i^k, \quad k = 0, \ldots, P. \tag{39}$$

For $m$ fast modes, we obtain the following simplified system

$$\dot{\boldsymbol{y}}^k \approx \sum_{i=m+1}^{n} \bar{\boldsymbol{a}}_i f_i^k = \underbrace{(I - \sum_{i=1}^{m} \bar{\boldsymbol{a}}_i \bar{\boldsymbol{b}}_i^T)}_{\bar{P}} \boldsymbol{g}^k =: \bar{P}\boldsymbol{g}^k. \tag{40}$$

Note that, presently, the projection operator $\bar{P}$ on the slow dynamics space is deterministic, and the same for *all* the stochastic modes of the solution. This has to be contrasted with the method developed above.

Also note that the present simplification calls for a re-interpretation of the criterion (34). Specifically, we need to insert the spectral representations for $f_i$ and $\boldsymbol{y}$ in the inequality (14). Similar to the approach used for Algorithm 2, we use following approximate criterion:

$$\left\langle \left(\bar{\tau}_{m+1} \sum_{i=1}^{m} \bar{\boldsymbol{a}}_{\boldsymbol{i}} f_i\right)^2 \right\rangle < \varepsilon_{rel} \left\langle \boldsymbol{y}^2 \right\rangle + \varepsilon_{abs} \mathbf{1}.$$

Note that the situation is simpler because $\bar{\tau}_{m+1} = 1/\bar{\lambda}_{m+1}$ and $\bar{\boldsymbol{a}}_i$ are deterministic. Recall that $(\bar{\lambda}_i, \bar{\boldsymbol{a}}_i)$ are the eigenpairs of the nominal system.

*4.2.1. Algorithm for the simplified CSP with nominal eigenvectors*

For a system with $m$ fast modes, Algorithm 3 can be used for integration of the simplified stochastic system $\dot{\boldsymbol{y}}^k = \bar{P}\boldsymbol{g}^k$, with time steps on the order of $\alpha\bar{\tau}_{m+1}$ with $0 < \alpha \lesssim 1$.

**Algorithm 3** One step of CSP integration (assuming modes $1, \ldots, m$ are fast) for the stochastic system using the nominal right eigenvectors as CSP vectors.

$\bar{\Lambda}(t) = \left[\bar{\Lambda}_{ij}(t)\right] = \left(\dot{\bar{\boldsymbol{b}}}_i^T + \bar{\boldsymbol{b}}_i^T \bar{J}\right) \bar{\boldsymbol{a}}_j \Big|_t$
$\bar{\Gamma}(t) = \left(\bar{\Lambda}(t)\right)^{-1}$
**for** $k = 0$ to $P$ **do**
  $\hat{\boldsymbol{y}}^k(t + \Delta t) = \boldsymbol{y}^k(t) + \int_t^{t+\Delta t} \bar{P}\boldsymbol{g}^k(\boldsymbol{y}(s))\, ds$ {Integration of the slow dynamics}
**end for**
$f_j^k(t) = \bar{\boldsymbol{b}}^j(t) \cdot \boldsymbol{g}^k\left[\hat{\boldsymbol{y}}(t + \Delta t)\right], \quad j = 1, \ldots, m, \quad k = 0, \ldots, P$
**for** $k = 0$ to $P$ **do**
  $\delta\boldsymbol{y}^k(t) = \sum_{i=1}^{m} \gamma_i^k(t) \bar{\boldsymbol{a}}_i(t), \quad$ where $\gamma_i^k(t) = \sum_{j=1}^{m} \bar{\Gamma}_{ij}(t) f_j^k(t)$
  $\boldsymbol{y}^k(t + \Delta t) = \hat{\boldsymbol{y}}^k(t + \Delta t) - \delta\boldsymbol{y}^k(t)$ {Radical correction}
**end for**

## 5. A model problem

In this section, we recall the 3-species model problem of Valorani et al. [42] and discuss its main properties in view of the CSP formalism. The deterministic problem is specified in section 5.1. Section 5.2 discusses the deterministic solution, illustrating the evolution of the mode amplitudes and the criterion determining the dimensionality of the fast subspace, given in (14). The Galerkin form of the stochastic system is then derived in section 5.3.

*5.1. The deterministic problem*

We consider the following nonlinear system [42]

$$\begin{cases} \dot{y}_1 &= -\dfrac{5y_1}{\varepsilon} - \dfrac{y_1 y_2}{\varepsilon} + y_2 y_3 + \dfrac{5y_2^2}{\varepsilon} + \dfrac{y_3}{\varepsilon} - y_1, \\ \dot{y}_2 &= \dfrac{10y_1}{\varepsilon} - \dfrac{y_1 y_2}{\varepsilon} - y_2 y_3 - \dfrac{10y_2^2}{\varepsilon} + \dfrac{y_3}{\varepsilon} + y_1, \\ \dot{y}_3 &= \dfrac{y_1 y_2}{\varepsilon} - y_2 y_3 - \dfrac{y_3}{\varepsilon} + y_1, \end{cases} \tag{41}$$

with small parameter $\varepsilon = 10^{-2}$. We shall refer to (41) as the VG model. The initial conditions are chosen to be

$$y_1(0) = y_2(0) = y_3(0) = 0.5. \tag{42}$$

The Jacobian of the source term with respect to the state variables, $y_i$, $i = 1, \ldots, 3$, is:

$$J = \begin{bmatrix} -\dfrac{5}{\varepsilon} - \dfrac{y_2}{\varepsilon} - 1 & -\dfrac{y_1}{\varepsilon} + y_3 + \dfrac{10y_2}{\varepsilon} & y_2 + \dfrac{1}{\varepsilon} \\ \dfrac{10}{\varepsilon} - \dfrac{y_2}{\varepsilon} + 1 & -\dfrac{y_1}{\varepsilon} - y_3 - \dfrac{20y_2}{\varepsilon} & -y_2 + \dfrac{1}{\varepsilon} \\ \dfrac{y_2}{\varepsilon} + 1 & \dfrac{y_1}{\varepsilon} - y_3 & -y_2 - \dfrac{1}{\varepsilon} \end{bmatrix}. \tag{43}$$

We shall simply refer to $J$ as the Jacobian of (41).

*5.2. CSP timescales*

Figure 1 (top) shows the evolution of the solution and of the system timescales. Note that the state vector tends towards a steady state, corresponding to the stable equilibrium point $y_i^* = 1$, $i = 1, \ldots, 3$. It is also evident that there is a pronounced disparity between the timescales of the system. In particular, the largest timescale is by more than three orders of magnitude larger than the remaining two, as depicted in Figure 1 (bottom). Hence, the system trajectory quickly approaches a one-dimensional manifold as the fastest two modes get exhausted. The time scale disparities makes this system well suited to CSP analysis, particularly to mitigate the corresponding stiffness and to alleviate the computational needs by allowing bigger explicit time steps.

Figure 2 shows the mode amplitudes, $f_i$, computed based on the right-hand side of (41). Both $f_1$ and $f_2$ exhibit a large drop, reaching values that are negligible compared to $f_3$. The figure also depicts the difference between the left-hand side and the right-hand side of the inequality (14), namely:

$$\boldsymbol{C}_{exh} = \tau_{m+1} \times |\sum_{i=1}^{m} \boldsymbol{a}_i f_i| - \varepsilon_{rel}|\boldsymbol{y}| - \varepsilon_{abs}\mathbf{1}. \tag{44}$$

for $m = 1$ and $m = 2$ (we used $\varepsilon_{rel} = 10^{-3}$ and $\varepsilon_{abs} = 10^{-10}$ in our computations). Note that, as before, in (44) the absolute value operator acts component-wise on vectors. Once all components of $\boldsymbol{C}_{exh}$ become negative, the mode is deemed exhausted. Hence, it can be inferred from this plot, that the first and second modes exhaust around $t = 3 \times 10^{-3}$ and $t = 2 \times 10^{-1}$ respectively.

*5.3. Galerkin formulation of the uncertain VG model*

Consider the system (41) introduced in section 5.1. We now assume that the rate parameter, $\varepsilon$, and the initial conditions are uncertain. Furthermore, we assume that these random variables are independent and uniformly distributed, namely according to:

$$y_1(0) = y_1^0 + \nu_1\xi_1, \quad y_2(0) = y_2^0 + \nu_2\xi_2, \quad y_3(0) = y_2^0 + \nu_3\xi_3, \quad \varepsilon^{-1} = \varepsilon_0^{-1} + \nu_4\xi_4,$$

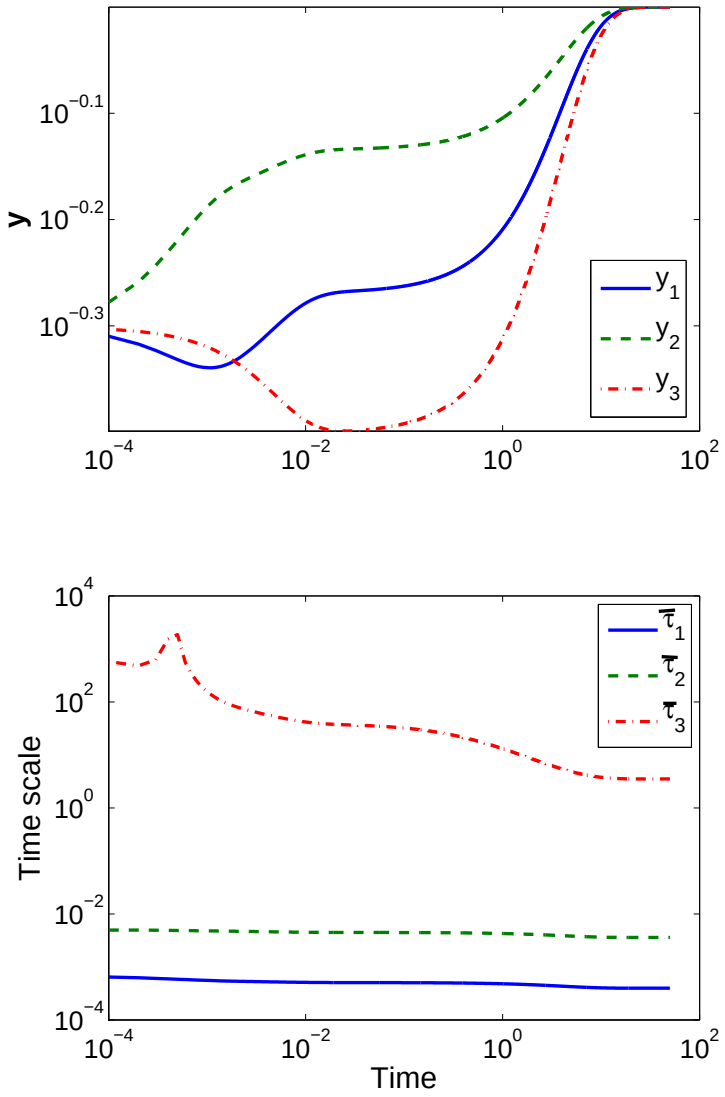


Figure 1: Evolution of the solution vector (top) and of the reaction time scales (bottom) for the deterministic system. The VG model is integrated using an explicit first-order scheme with $\Delta t = 10^{-4}$.

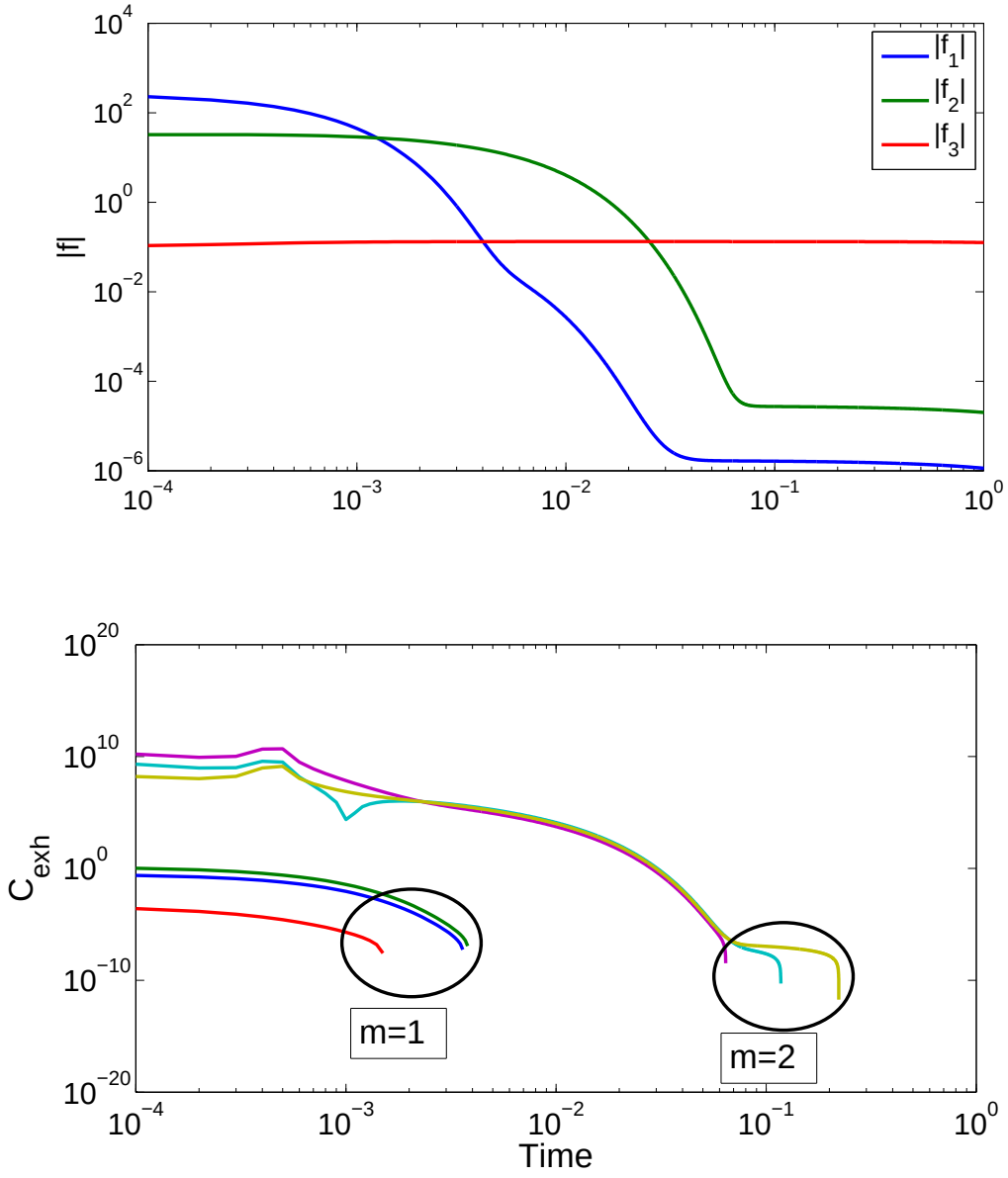


Figure 2: Top: Evolution of the modes amplitudes $|f_i|$. Bottom: evolution of index $\boldsymbol{C}_{exh}$ defined in (44), for the deterministic solution shown in Fig. 1.

where $\xi_i \overset{iid}{\sim} \mathcal{U}(-1,1)$, $i = 1,\dots,4$. Thus, we work in the probability space $(\Omega^*, \mathcal{B}(\Omega^*), F_{\boldsymbol{\xi}})$ as introduced in section 2. In the present case case we have $\Omega^* = [-1,1]^4$, and the expected value of the random vector $\boldsymbol{\xi} = (\xi_1,\dots,\xi_4)$ is $\bar{\boldsymbol{\xi}} = \mathbf{0}$.

In our numerical experiments, we choose the nominal values for $y_1^0$, $y_2^0$, and $y_3^0$ as in (42) and $\varepsilon_0^{-1} = 100$ (also the nominal value), and use the following sets of values for $\nu_1$, $\nu_2$, $\nu_3$, and $\nu_4$:

$$\nu_1 = \nu_2 = \nu_3 = 0.02, \quad \nu_4 = 1, \tag{45}$$

$$\nu_1 = \nu_2 = \nu_3 = 0.2, \quad \nu_4 = 10. \tag{46}$$

To illustrate the effect of randomness on the system trajectory, we select a small sample of random parameters corresponding to ranges of uncertainty given through (45), and plot in Figure 3(a) realizations of $y_i(t,\boldsymbol{\xi})$, and in Figure 3(b) the realizations in phase space. Note that as time increases, all trajectories converge to the same (deterministic) equilibrium point, and that the uncertainty amplitude decreases.

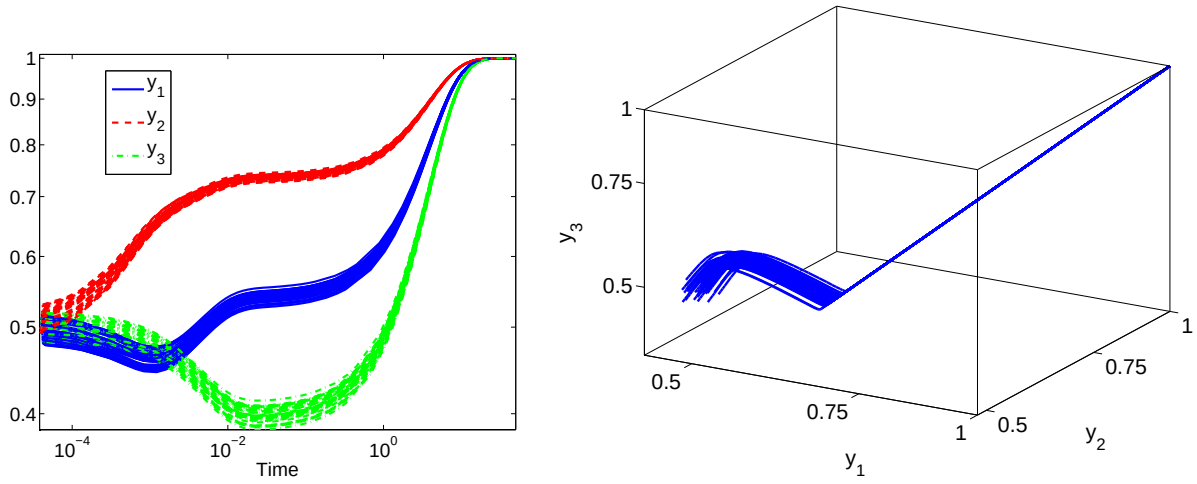


Figure 3: Realizations of the uncertain dynamics: (a) evolution of $y_i(t,\boldsymbol{\xi})$; (b) trajectories in phase-space. These plots correspond to the case of $\nu_1 = \nu_2 = \nu_3 = 0.02, \nu_4 = 1$.

As discussed in section 2.4, we seek to find the projection of the system trajectory in $(\mathcal{V}^p)^n$:

$$y_i = \sum_{k=0}^{P} y_i^k \Psi_k, \tag{47}$$

where the $\Psi_k$ presently denote 4D Legendre polynomials in the random variables $\xi_1,\dots,\xi_4$. The Galerkin system for (41) is given by:

$$\begin{cases} \dot{y}_1^k = -\left(\dfrac{5}{\varepsilon_0}+1\right) y_1^k + \dfrac{y_3^k}{\varepsilon_0} + \nu_4\left(\mathcal{M}_3^\xi - 5\mathcal{M}_1^\xi + 5\mathcal{M}_{22}^\xi - \mathcal{M}_{12}^\xi\right) + \dfrac{1}{\varepsilon_0}\left(5\mathcal{M}_{22} - \mathcal{M}_{12}\right) + \mathcal{M}_{23}, \\ \dot{y}_2^k = \left(\dfrac{10}{\varepsilon_0}+1\right) y_1^k + \dfrac{y_3^k}{\varepsilon_0} + \nu_4\left(10\mathcal{M}_1^\xi + \mathcal{M}_3^\xi - \mathcal{M}_{12}^\xi - 10\mathcal{M}_{22}^\xi\right) - \dfrac{1}{\varepsilon_0}\left(\mathcal{M}_{12} + 10\mathcal{M}_{22}\right) - \mathcal{M}_{23}, \\ \dot{y}_3^k = \dfrac{1}{\varepsilon_0}\left(y_1^k - y_3^k\right) + \nu_4\left(\mathcal{M}_{12}^\xi - \mathcal{M}_3^\xi\right) - \dfrac{1}{\varepsilon_0}\mathcal{M}_{12} - \mathcal{M}_{23}, \end{cases} \tag{48}$$

where the factors $\mathcal{M}$ are given by:

$$\mathcal{M}_1^\xi = \frac{1}{\langle\Psi_k^2\rangle}\sum_{i=0}^{P} y_1^i\langle\xi_4\Psi_i\Psi_k\rangle, \qquad \mathcal{M}_3^\xi = \frac{1}{\langle\Psi_k^2\rangle}\sum_{i=0}^{P} y_3^i\langle\xi_4\Psi_i\Psi_k\rangle,$$

$$\mathcal{M}_{12} = \frac{1}{\langle\Psi_k^2\rangle}\sum_{i=0}^{P}\sum_{j=0}^{P} y_1^i y_2^j\langle\Psi_i\Psi_j\Psi_k\rangle, \qquad \mathcal{M}_{12}^\xi = \frac{1}{\langle\Psi_k^2\rangle}\sum_{i=0}^{P}\sum_{j=0}^{P} y_1^i y_2^j\langle\xi_4\Psi_i\Psi_j\Psi_k\rangle,$$

$$\mathcal{M}_{23} = \frac{1}{\langle\Psi_k^2\rangle}\sum_{i=0}^{P}\sum_{j=0}^{P} y_2^i y_3^j\langle\Psi_i\Psi_j\Psi_k\rangle, \qquad \mathcal{M}_{22} = \frac{1}{\langle\Psi_k^2\rangle}\sum_{i=0}^{P}\sum_{j=0}^{P} y_2^i y_2^j\langle\Psi_i\Psi_j\Psi_k\rangle,$$

$$\mathcal{M}_{22}^\xi = \frac{1}{\langle\Psi_k^2\rangle}\sum_{i=0}^{P}\sum_{j=0}^{P} y_2^i y_2^j\langle\xi_4\Psi_i\Psi_j\Psi_k\rangle.$$

Thus, due to the simple structure of the system, involving single, double, or triple products of random variables, a true Galerkin approximation has been used. In other words, the need for approximate (pseudo-spectral) evaluations [6] of PC transforms has been avoided. Below, solutions of (48) obtained using small explicit time steps will be contrasted to numerical solutions obtained using the simplified stochastic CSP acceleration.

## 6. Numerical computations

Since the CSP method involves the calculation of the system eigenvalues and eigenvectors, it is crucial first to quantify and analyze the effect of uncertainty on these entities in order to justify the choice of the CSP vectors. Hence, we first start in Section 6.1 by conducting a numerical study of the effect of uncertainty using the measures defined in Section 3.4. We also provide a brief description of the evolution of this uncertainty as a function of time. Secondly, we provide in Section 6.1.2 a comparison between NISP and residual minimization approaches for computing the eigenvalues and eigenvectors of the stochastic system Jacobian. In Section 6.2, we compute the stochastic mode amplitudes $f$. Finally, we compare and validate the CSP integrator using the two algorithms described in Section 4. We also briefly discuss the performance of our proposed CSP method versus explicit, small time step, integration of the Galerkin system.

### *6.1. Computation and analysis of the Stochastic Eigenvectors*

In this section, we study the effects of the uncertainty on the eigenstructure of the system Jacobian. We present results for low and moderate ranges of initial uncertainty and show the effect of randomness first at $t = 0$ and then track the effect of randomness on fast and slow system manifolds over time. We also briefly examine the convergence of the predictions as a function of the order of the PC expansion.

#### *6.1.1. The situation at $t = 0$*

Here we analyze the impact of uncertainty at the initial time. Figure 4 shows the corresponding PDFs for the $\eta(\boldsymbol{\xi}) = \|H(\boldsymbol{\xi}) - I\|_F$ at $t = 0$. These were generated using the NISP approach. Recall that $\eta(\boldsymbol{\xi})$ measures the deviation of the stochastic eigenvectors from those of the nominal system. We notice that the support of the PDFs of $\eta$ shift to the right as the level of uncertainty increases, consistently with the corresponding values of $\nu_i$.

Figure 5 shows the distribution of $\cos(\zeta_i(\boldsymbol{\xi}))$ at $t = 0$, which quantifies the inclination of stochastic eigenvectors $\boldsymbol{a}_i(\boldsymbol{\xi})$ with respect to their "nominal" counterparts. The support of the PDFs of $\cos(\zeta_i(\boldsymbol{\xi}))$ is in the neighborhood of 1, *i.e.* $\zeta_i \approx 0$, for both levels of uncertainty considered. This implies that the uncertainty has a weak effect on the orientation of the stochastic eigenvectors as they remain essentially aligned with the corresponding eigenvectors of the nominal system. Figure 6 depicts the distributions of the eigenvalues at $t = 0$. Note in particular that the slowest mode of the system, corresponding to $\lambda_3$, shows a large range of uncertainty in the case of $\nu_1 = \nu_2 = \nu_3 = 0.2$ and $\nu_4 = 10$. Furthermore, a smaller level of uncertainty results in a tighter PDF for all $\lambda_i$.

For all quantities considered, $\eta(\boldsymbol{\xi})$, $\cos(\zeta_i(\boldsymbol{\xi}))$, and $\lambda_i(\boldsymbol{\xi})$, the results show general convergence of the predictions as the PC order increases, albeit with small changes in the $|\lambda_3|$ PDF still evident in going from second to third order PC for the higher uncertainty case. Allowing for these minor differences, we may say

that at least a second order expansion is required to capture the large-scale structure the PDFs at the start of the computations. Based on the behavior of the stochastic system, illustrated in Fig. 3, the uncertainty level is expected to decrease as a function of time, which indicates that the expansion order does not need to be increased as the system evolves. Therefore, in all the simulations below we use a PC expansion order $No = 2$.

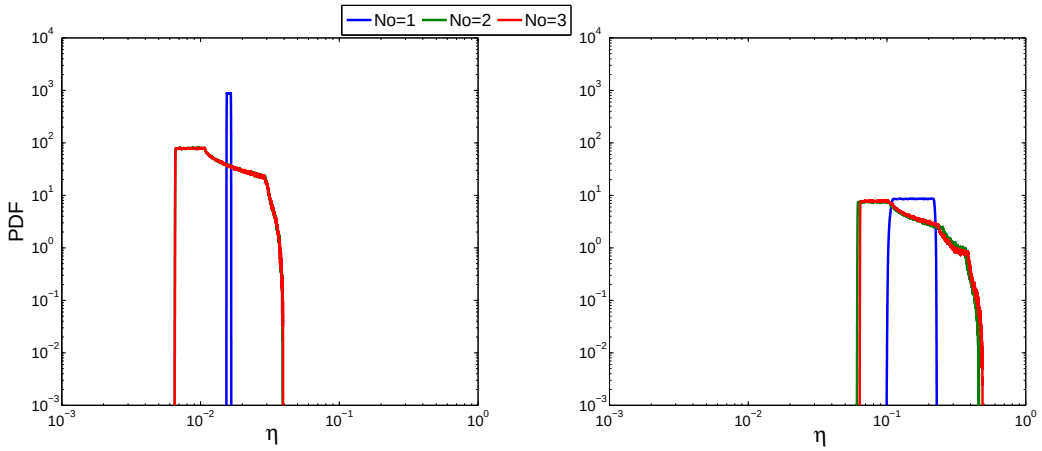


Figure 4: PDFs of $\eta$ at time $t = 0$. Left: $\nu_1 = \nu_2 = \nu_3 = 0.02$ and $\nu_4 = 1$; right: $\nu_1 = \nu_2 = \nu_3 = 0.2$ and $\nu_4 = 10$. The curves are generated using NISP with 10 Gauss quadrature points and different expansion orders ($No$), as indicated.

*6.1.2. Comparison between NISP and residual minimization*

To assess the validity of our results, we compare the eigenvalues and eigenvectors of the stochastic system computed using NISP (Section 2.4.1) and the residual minimization (Section 3.3) approaches. The PC coefficients of the eigenvalues $\lambda_i$ computed using both approaches are compared in Figure 7. We compare the respective deviations of the eigenvectors from their nominal counterparts in Figure 8 where we show the spectral coefficients of $\cos(\zeta_i)$ computed via NISP and residual minimization. Finally, in Figure 9, we compare the spectral representations of $h_{ij}(\boldsymbol{\xi})$ estimated using both methods. In all cases, a very good agreement between the two methods is observed.

From Figure 7, we see that the the stochastic eigenvalues exhibit a somewhat broad spectrum, with significant "energy" in the higher modes. This implies that uncertainty has a significant effect on the stochastic system timescales. On the other hand, the spectrum of $\cos(\zeta_i)$ exhibits an essentially degenerate structure, with order-of-magnitude differences between the amplitude of the mean, which remains close to 1, and that of higher modes. This is consistent with the support of the PDFs in Figure 5. The spectra of the $h_{ii}$, depicted in Figure 9, follow a similar trend to those of $\cos(\zeta_i)$ with a mean close to 1 and very low amplitudes for the higher modes. Moreover, all the amplitudes of $h_{i\neq j}$ are very small. These findings imply that for the present system, the eigenvectors are much less affected by uncertainty than the eigenvalues, which motivates the present simplified CSP approach, including the use of deterministic nominal eigenvectors.

*6.1.3. Evolution of uncertainty over time*

Figure 10 shows the time evolution of the distribution of $\eta(\boldsymbol{\xi})$. The results show that, as expected, the range of uncertainty in the eigenvectors of the stochastic system Jacobian becomes smaller as time increases. However, we note that the uncertainty in $\eta$ continues to be present even in large time, even though the system has essentially reached a deterministic steady state. Thus, even at the equilibrium, the impact of uncertainty does not totally vanish. This is a reflection of the fact that, whereas the equilibrium point is independent of $\boldsymbol{\xi}$, the Jacobian of the system at the equilibrium point remains a stochastic quantity, namely due the assumed uncertainty in the rate $\epsilon$.

*6.2. Stochastic system timescales*

To get further insight into the effect of uncertainty, we consider the evolution of the amplitudes, $f_i$, appearing in the eigenvector decomposition of the stochastic source term. The PC representations of these amplitudes are given by:

$$f_i = \sum_{k=0}^{P} f_i^k \Psi_k$$

and the absolute values of the coefficients $|f_i^k|$ are plotted in Figure 11. We note that only mode $f_3^0$ corresponding to the zeroth order (mean) of the slowest physical time scale, preserves a relatively high amplitude compared to the other modes. This mode is closely related to the slow reaction time scale $\bar{\tau}_3$ of the deterministic system illustrated in Figure 1. Furthermore, $|f_3^0|$ is comparable to the third mode of the deterministic system $f_3$ (Figure 2). This result is not surprising because, as discussed in Section 6.1.2, the eigenvectors $\boldsymbol{b}_i$ are weakly affected by the uncertainty. This further motivates the use of the nominal eigenvectors in the simplified CSP analysis.

*6.3. Validation of the stochastic CSP integrator*

We implemented the two simplified CSP approaches described in Section 4 to efficiently integrate the stochastic Galerkin system. Figure 12 shows the mean trajectory along with two standard deviation bounds (dotted lines) for the species of the system discussed in Section 5. Shown are results computed using explicit integration with small $\Delta t$, and the two simplified CSP algorithms. The figures reveal close correspondence between the different predictions. In particular, there is a close agreement in the solution transients, and in all cases the stable deterministic equilibrium is reached.

To quantify the differences between the predictions, we rely on the $L^2$ norms defined below. Since the system components exhibit similar behavior, we focus on the first component $y_1(t, \boldsymbol{\xi})$. To simplify the notation, we shall use $Y$ to denote the component $y_1$ obtained via explicit, small time step, integration of the Galerkin system, $\tilde{Y}$ the corresponding prediction obtained using Algorithm 2, and $\hat{Y}$ the estimate computed via Algorithm 3.

We first check the accuracy of the Galerkin approximation by computing the relative error:

$$E(t) = \frac{\|y(t,\cdot) - Y(t,\cdot)\|_{L^2(\Omega^*)}}{\|y(t,\cdot)\|_{L^2(\Omega^*)}}. \tag{49}$$

where the norms were approximated via Monte Carlo integration. In other words, we pick a sample $S \subseteq \Omega^*$ and estimate $E$ according to:

$$E(t) \approx \frac{\left(\frac{1}{|S|}\sum_{\boldsymbol{q}\in S} |y(t,\boldsymbol{q}) - Y(t,\boldsymbol{q})|^2\right)^{1/2}}{\left(\frac{1}{|S|}\sum_{\boldsymbol{q}\in S} |y(t,\boldsymbol{q})|^2\right)^{1/2}},$$

where $|S|$ denotes the number of elements in $S$. Note that for a fixed $\boldsymbol{q} \in S$, $y(t,\boldsymbol{q})$ is the solution of a deterministic problem. In Table 1, we report $E(t)$ for selected values of $t$. Note that the relative error is less than 0.1%, which signifies a very good agreement between the explicit Galerkin solution and the Monte Carlo solution. Next, we test the validity of Algorithm 2 and Algorithm 3 by computing the following relative $L^2(\Omega^*)$ errors,

$$\tilde{E}(t) = \frac{\left\|Y(t,\cdot) - \tilde{Y}(t,\cdot)\right\|_{L^2(\Omega^*)}}{\|Y(t,\cdot)\|_{L^2(\Omega^*)}}, \qquad \hat{E}(t) = \frac{\left\|Y(t,\cdot) - \hat{Y}(t,\cdot)\right\|_{L^2(\Omega^*)}}{\|Y(t,\cdot)\|_{L^2(\Omega^*)}}, \tag{50}$$

| $t$ | $E(t)$ |
|---|---|
| $10^{-2}$ | $6.28 \times 10^{-4}$ |
| $10^{-1}$ | $2.15 \times 10^{-5}$ |
| $10^{0}$ | $8.06 \times 10^{-4}$ |
| $10^{1}$ | $2.23 \times 10^{-4}$ |

Table 1: Relative $L^2$ error between the Galerkin approximation (with a second order PC expansion) and the Monte Carlo solution. Results correspond to $\nu_1 = \nu_2 = \nu_3 = 0.02$ and $\nu_4 = 1$.

which quantify the distance between the respective CSP estimates and the numerical solution obtained using small time step integration. Note that computing these norms is straightforward because the PC expansions of $Y$, $\hat{Y}$, and $\tilde{Y}$ are readily available. For instance, we have:

$$\left\| Y(t,\cdot) - \tilde{Y}(t,\cdot) \right\|_{L^2(\Omega^*)} = \Big[ \sum_{k=0}^{P} \left( Y^k(t) - \tilde{Y}^k(t) \right)^2 \left\langle \Psi_k^2 \right\rangle \Big]^{1/2}. \tag{51}$$

Figure 13 shows the evolution of the norms $\hat{E}(t)$ and $\tilde{E}(t)$. Overall, the relative error is found to be very small ($\sim 10^{-4}$). The results also indicate that for small and intermediate times ($t < 10$) $\tilde{E}$ rises faster than $\hat{E}$, even though spectral representation of the stochastic eigenvectors is used in Algorithm 2 whereas deterministic nominal eigenvectors are used in Algorithm 3. This is likely due to spectral truncation errors associated with Galerkin divisions and the stochastic matrix inversion featuring in Algorithm 2. Note however, that in both cases the peaks are of comparable magnitude, and that at large time both $\hat{E}(t)$ and $\tilde{E}(t)$ drop rapidly and assume nearly identical values. Thus, for the present system, the CSP integration errors appear to be bounded, and tend to become asymptotically small as the deterministic equilibrium point is approached. Note that the errors in Figure 13 are computed with the order of the PC expansion fixed at $No = 2$. Repeating the error analysis with $No = 3$ and $No = 4$ gave nearly identical error plots. This implies that the PC truncation errors incurred in both algorithms are insignificant in comparison to the (small) CSP reduction errors.

### *6.4. Performance of the stochastic CSP integrator*

Here we quantify the performance of our CSP integrator as compared to explicit, small time-step, integration of the Galerkin system. In Table 2, we report the CPU times required by explicit and CSP integration of (8). The simulations were performed on an Intel Core I7 machine operating at 2.66 Ghz with 8Gb of RAM. Note that as the expansion order is increased, the Galerkin system size, $N$, becomes larger according to $N = n\dfrac{(M+No)!}{M!No!}$, where $n$ is the dimension of the corresponding deterministic system, $M$ is the number of random parameters, and $No$ is the expansion order. As indicated in Table 2, as $No$ increases, the Galerkin system size also increases. In our model problem, $n = 3$ and $M = 4$, so with a fourth-order expansion $N = 210$, a size that is representative of large deterministic chemical kinetic systems.

We first notice the order-of-magnitude speedup when using Algorithm 3. To place the estimates in perspective, we note that in both the Galerkin system (48) and the CSP projected system (40) have the same size $n \times (P+1)$. Thus, an upper estimate of the speedup associated with CSP may be obtained from the ratio of the number integration steps required by both methods to advance the solution to the same final time. With Algorithm 3 only 8200 time steps are needed to integrate the system to $t = 50$, whereas with explicit integration of the Galerkin system $5 \times 10^5$ time steps are required. This translates to a ratio of about 61 which is close to the speedup values reported in Table 2 for Algorithm 3. Thus, for Algorithm 3,the CSP operations do not incur significant overhead.

The speedup observed for Algorithm 2 is substantially lower than that of Algorithm 3. This is due to the additional computational costs required by Algorithm 2, namely by additional Galerkin products, Galerkin divisions, the computation of the stochastic eigenvectors $\boldsymbol{a}_i$ and $\boldsymbol{b}_i$, and the inversion of the stochastic matrix $\Lambda$. For the present small system, these additional overheads make Algorithm 2 mildly attractive. However,

as the expansion order is increased, we observe an increasing speed-up, suggesting that performance of Algorithm 2 increases with the dimension of the PC basis. Moreover, for larger systems, the overheads associated with stochastic matrix inversion may be dominated by source term evaluations. In these situations, Algorithms 2 and 3 would be expected to exhibit comparable performance.

| Expansion order | No=1 | No=2 | No=3 | No=4 |
|---|---|---|---|---|
| System size | 15 | 45 | 105 | 210 |
| Explicit integration CPU time | 0.2 | 1.63 | 13.7 | 108.34 |
| Algorithm 2 CPU time | 0.22 (0.91) | 0.49 (3.32) | 2.14 (6.4) | 15.07 (7.19) |
| Algorithm 3 CPU time | 0.0034 (58.8) | 0.027 (60.4) | 0.23 (59.6) | 1.77 (61.2) |

Table 2: CPU time in minutes of the integration of VG model with different methods for a total simulation time $t_{total} = 50$. The speedup gained by CSP is shown in parentheses.

## 7. Conclusions

In this paper we have applied CSP to address stiffness in a dynamical system with parametric uncertainty. We relied on PC expansions to represent the uncertain inputs and the system response. Specifically, a Galerkin formalism was used to derive an expanded ODE system that governs the evolution of the PC coefficients of the state variables.

Attention was focused on the case of a dynamical system that has distinct, well separated, timescales, and that tends to a deterministic steady state irrespective of the values of the random inputs. A simplified CSP methodology was developed based on a detailed analysis of eigenvalues and eigenvectors of the stochastic system Jacobian. The latter provided a relationship between the PC representation of the Jacobian of the underlying uncertain system and the Jacobian of Galerkin form of the stochastic system. Based on the PC representation of the stochastic eigenvalues, and the spectral representation of the eigenvectors *in state space*, two simplified CSP algorithms were developed. The first exploits the PC representation of the stochastic eigenvectors to describe the dependence of fast and slow manifolds on random variables that are used to parametrize the random inputs. In the second algorithm, the fast and slow manifolds are described in terms of the deterministic eigenvectors associated with a nominal system.

Computational experiments were conducted to illustrate the eigenvector representations and to test the performance of the simplified CSP integrator algorithms. The analysis showed that for the present system, the stochastic eigenvalues exhibit a rich PC spectrum and accordingly pronounced variability, whereas the eigenvectors exhibit an essentially degenerate spectrum with the dominant amplitude lying in the mean. Thus, the random eigenvectors were found to remain closely aligned with the corresponding nominal ones, which supports the use of a simplified CSP projection onto deterministic (nominal) manifolds. While this is, of course, not guaranteed in general, the present approach provides a feasible handle on a first-cut analysis of uncertain ODE dynamics. The analysis of a general system using this method provides useful insights into the major features of the underlying dynamics.

The simulations were also used to validate the explicit Galerkin solution, namely by comparison with direct Monte Carlo integration. The validated Galerkin solution was then used to test the performance of the simplified CSP algorithms. In all cases, a close agreement between the predictions was found, and substantial speedup in the integration of the uncertain dynamical system was obtained. In particular, when CSP using nominal eigenvectors was used, order-of-magnitude improvements in integration efficiency were observed.

While the simulations conducted in this paper focused on a simplified stiff system, the analysis and computational experiments point to several potential extensions of the present stochastic reduction methodology. One avenue concerns the generalization of the stochastic Jacobian analysis, and the associated characterization of the fast and slow manifolds. In the computations, we have exploited the fact that the spectrum of the stochastic Jacobian revealed distinct real eigenvalues, and consequently relied on pairwise comparison of stochastic eigenvectors. It appears possible to extend this approach so that one characterizes directly

the dependence of the fast and slow stochastic manifolds on the uncertainty germ. By doing so, it may be possible to also capture the situation where fast eigenvectors exhibit substantial sensitivity to the uncertain parameters, but that the corresponding manifold remains weakly sensitive to these parameters. This may be possibly accomplished by developing metrics that account for the angles between stochastic subspaces; implementation of such metrics would enable us to adapt the present algorithms to more complex conditions.

A second avenue that we also plan to explore is to consider ignition problems, which generally exhibit large positive eigenvalues in route towards chemical equilibrium. In these problems, the impact of input uncertainties would generally not be expected to decay asymptotically, as was the case in the present model problem. Consequently, a more detailed analysis may be required to assess the performance of the stochastic reduction algorithm, and if necessary refine the implementation of CSP exhaustion criteria.

By considering a more general suite of ignition problems, we also plan to investigate and establish criteria under which a deterministic reduction approach would be valid, e.g. in light of user-defined tolerances. It is anticipated that such analyses would lead to robust guidelines under which deterministic projections would be valid, and to extended algorithms for dynamically selecting between deterministic and stochastic reduction schemes.

## A. Stochastic matrix inversion

Let $A \in \mathbb{R}^{n\times n}$ be a non-singular matrix. The following Newton iteration for computing the inverse of $A$ is well known [3, 4, 7, 33]:

$$X_{n+1} = X_n(2I - AX_n).$$

As stated in [3, 4, 7] to ensure convergence, $X_0$ is specified by

$$X_0 = \kappa A^T, \quad \text{with } \kappa \in (0, \frac{2}{\lambda_1}), \text{ where } \lambda_1 \text{ is the largest eigenvalue of } AA^T. \tag{52}$$

For the case of a stochastic matrix $A \in (\mathcal{V}^p)^{n\times n}$, the Galerkin formulation of the above iteration is given by,

$$X_{n+1} = X_n \circledast (2I - A \circledast X_n).$$

Guided by (52), we choose the initial guess through

$$X_0^0 = \kappa \times (A^0)^T, \quad X_0^k = 0, \quad k = 1, \ldots P.$$

where $0 < \kappa < 2/\lambda_1$ and $\lambda_1$ is the largest eigenvalue of $A^0(A^0)^T$. In the computations in the present paper, this iterative method was found to be very effective in providing an approximation to the spectral representation of the stochastic matrix inverse.

## References


[1] M. Abramowitz and I.A. Stegun. *Handbook of Mathematical Functions.* Dover, 1970.

[2] A. Alexanderian, O.P. Le Maître, H.N. Najm, M. Iskandarani, and O.M. Knio. Multiscale stochastic preconditioners in non-intrusive spectral projection. *Journal of Scientific Computing*, pages 1–35, 2011. 10.1007/s10915-011-9486-2.

[3] A. Ben-Israel. An iterative method for computing the generalized inverse of an arbitrary matrix. *Math. Comp.*, 19:452–455, 1965.

[4] A. Ben-Israel and D. Cohen. On iterative computation of generalized inverses and associated projections. *SIAM J. Numer. Anal.*, 3:410–419, 1966.

[5] R.H. Cameron and W.T. Martin. The orthogonal development of nonlinear functionals in series of Fourier-Hermite functionals. *Annals of Mathematics*, 48:385–392, 1947.

[6] B.J. Debusschere, H.N. Najm, P.P. Pébray, O.M. Knio, R.G. Ghanem, and O.P. Le Maître. Numerical challenges in the use of Polynomial Chaos representations for stochasic processes. *SIAM J. Sci. Comp.*, 26:698–719, 2004.

[7] H.P. Decell, Jr. and S.W. Kuhng. An iterative method for computing the generalized inverse of a matrix. Report D-3464, NASA TN, 1966.

[8] C.G. Fotache, T.G. Kreutz, and C.K. Law. Ignition of Counterflowing Methane versus Heated Air under Reduced and Elevated Pressures. *Combustion and Flame*, 108:442–470, 1997.

[9] R. Ghanem and D. Ghosh. Efficient characterization of the random eigenvalue problem in a polynomial chaos decomposition. *International Journal of Numerical Methods in Engineering*, 72:486–504, 2007.
[10] R.G. Ghanem and P.D. Spanos. A spectral stochastic finite element formulation for reliability analysis. *J. Eng. Mech. ASCE*, 117:2351–2372, 1991.
[11] R.G. Ghanem and P.D. Spanos. *Stochastic Finite Elements: A Spectral Approach*. Springer Verlag, 1991.
[12] D.A. Goussis. On the Construction and Use of Reduced Chemical Kinetics Mechanisms Produced on the Basis of Given Algebraic Relations. *J. Comput. Physics*, 128:261–273, 1996.
[13] D.A. Goussis and S.H. Lam. A study of homogeneous methanol oxidation kinetic using csp. *Proc. Comb. Inst.*, 24:113–120, 1992.
[14] D.A. Goussis, M. Valorani, F. Creta, and H.N. Najm. Reactive and Reactive/Diffusive Time Scales in Stiff Reaction-Diffusion Systems. *Progress in Computational Fluid Mechanics*, 5(6):316–326, 2005.
[15] R.A. Horn and C.R. Johnson. *Matrix analysis*. Cambridge University Press, Cambridge, 1990.
[16] S. Janson. *Gaussian Hilbert Spaces*. Cambridge University Press, 1997.
[17] O. Kallenberg. *Foundations of Modern Probability*. Springer, second edition, 2002.
[18] A. Kazakov, M. Chaos, Z. Zhao, and F.L. Dryer. Computational Singular Perturbation Analysis of Two-Stage Ignition of Large Hydrocarbons. *J. Phys. Chem. A*, 110:7003–7009, 2006.
[19] S.H. Lam. Singular perturbation for stiff equations using numerical methods. In C. Casci, editor, *Recent Advances in the Aerospace Sciences*, page 3. Plenum Press, New York, 1985.
[20] S.H. Lam. Using CSP to Understand Complex Chemical Kinetics. *Combustion Science and Technology*, 89:375–404, 1993.
[21] S.H. Lam and D.A. Goussis. Understanding complex chemical kinetics with computational singular perturbation. *Proc. Comb. Inst.*, 22:931–941, 1988.
[22] S.H. Lam and D.A. Goussis. The CSP Method for Simplifying Kinetics. *International Journal of Chemical Kinetics*, 26:461–486, 1994.
[23] P.D. Lax. *Linear Algebra*. Wiley-Interscience, 1996.
[24] O.P. Le Maître and O.M. Knio. *Spectral Methods for Uncertainty Quantification with Applications to Computational Fluid Dynamics*. Springer, 2010.
[25] O.P. Le Maître, O.M. Knio, H.N. Najm, and R.G. Ghanem. A stochastic projection method for fluid flow. I. Basic formulation. *Journal of Computational Phyics*, 173:481–511, 2001.
[26] O.P. Le Maître, H.N. Najm, P.P. Pébay, R.G. Ghanem, and O.M. Knio. Multi-resolution-analysis scheme for uncertainty quantification in chemical systems. *SIAM J. Sci. Comput.*, 29(2):864–889, 2007.
[27] O.P. Le Maître, M.T. Reagan, H.N. Najm, R.G. Ghanem, and O.M. Knio. A stochastic projection method for fluid flow II. Random process. *J. Comput. Phys.*, 181:9–44, 2002.
[28] T.F. Lu, Y.G. Ju, and C.K. Law. Complex CSP for chemistry reduction and analysis. *Combustion and Flame*, 126:1445–1455, 2001.
[29] T.F. Lu and C.K. Law. A criterion based on computational singular perturbation for the identification of quasi steady state species: A reduced mechanism for methane oxidation with NO chemistry. *Combustion and Flame*, 154:761–774, 2008.
[30] C.D. Meyer. *Matrix Analysis and Applied Linear Algebra*. SIAM, 2001.
[31] H.N. Najm. Uncertainty quantification and polynomial chaos techniques in computational fluid dynamics. *Ann. Rev. Fluid Mech.*, 41:35–52, 2009.
[32] H.N. Najm, B.J. Debusschere, Y.M. Marzouk, S. Widmer, and O.P. Le Maître. Uncertainty Quantification in Chemical Systems. *Int. J. Num. Meth. Eng.*, 80:789–814, 2009.
[33] V. Olshevsky and E. Tyrtyshnikov, editors. *Matrix Methods: Theory, algorithms and applications dedicated to the memory of Gene Golub*. World scientific publishing, 2010.
[34] M. Rathinam and L. R. Petzold. A new look at proper orthogonal decomposition. *SIAM Journal on Numerical analysis*, 41:1893 – 1925, 2003.
[35] M.T. Reagan, H.N. Najm, R.G. Ghanem, and O.M. Knio. Uncertainty quantification in reacting flow simulations through non-intrusive spectral projection. *Combustion and Flame*, 132:545–555, 2003.
[36] B.E. Sonday, R.D. Berry, H.N. Najm, and B.J. Debusschere. Stochastic Eigenvalue Analysis. *SIAM J. Sci. Comp.*, 2011. in press.
[37] J. Tryoen, O.P. Le Maître, M. Ndjinga, and A. Ern. Intrusive galerkin methods with upwinding for uncertain nonlinear hyperbolic systems. *J. Computational Physics*, 228(18):6485–6511, 2010.
[38] M. Valorani, F. Creta, F. Donato, H.N. Najm, and D.A. Goussis. Skeletal Mechanism Generation and Analysis for $n$-heptane with CSP. *Proc. Comb. Inst.*, 31:483–490, 2007.
[39] M. Valorani, F. Creta, D.A. Goussis, J.C. Lee, and H.N. Najm. Chemical Kinetics Simplification via CSP. *Combustion and Flame*, 146:29–51, 2006.
[40] M. Valorani and D.A. Goussis. Explicit Time-Scale Splitting Algorithm For Stiff Problems: Auto-Ignition Of Gaseous-Mixtures Behind A Steady Shock. *J. Comput. Phys.*, 169:44–79, 2001.
[41] M. Valorani, D.A. Goussis, F. Creta, and H.N. Najm. Higher Order Corrections in the Approximation of Low Dimensional Manifolds and the Construction of Simplified Problems with the CSP Method. *J. Comput. Phys.*, 209:754–786, 2005.
[42] M. Valorani, D.A. Goussis, F. Creta, and H.N. Najm. Higher order corrections in the approximation of low-dimensional manifolds and the construction of simplified problems with the csp method. *J. Comput. Phys.*, 209:754–786, 2005.
[43] M. Valorani, H.N. Najm, and D. Goussis. CSP Analysis of a Transient Flame-Vortex Interaction: Time Scales and Manifolds. *Combustion and Flame*, 134(1-2):35–53, 2003.
[44] M. Valorani, S. Paolucci, and H.N. Najm. Sensitivity indices based on the *G-Scheme*. $2^{nd}$ Int. Workshop on Model

Reduction in Reacting Flows, Univ. of Notre Dame, Mar. 30–Apr. 9, 2009.
[45] N. Wiener. The homogeneous chaos. *Am. J. Math.*, 60:897–936, 1938.
[46] D. Williams. *Probability with martingales*. Cambridge Mathematical Textbooks. Cambridge University Press, Cambridge, 1991.
[47] D.B. Xiu and G.E. Karniadakis. The Wiener-Askey Polynomial Chaos for stochastic differential equations. *SIAM J. Sci. Comput.*, 24:619–644, 2002.
[48] D.B. Xiu and G.E. Karniadakis. Modeling uncertainty in flow simulations via generalized Polynomial Chaos. *Journal of Computational Physics*, 187:137–167, 2003.

## ACKNOWLEDGMENT

This work was supported by the US Department of Energy (DOE) under Award Number DE-SC0001980. HNN was supported by the DOE Office of Basic Energy Sciences (BES) Division of Chemical Sciences, Geosciences, and Biosciences. Sandia National Laboratories is a multiprogram laboratory operated by Sandia Corporation, a Lockheed Martin Company, for the United States Department of Energy under contract DE-AC04-94-AL85000. This report was prepared as an account of work sponsored in part by an agency of the United States Government. Neither the United States Government nor any agency thereof, nor any of their employees, makes any warranty, express or implied, or assumes any legal liability or responsibility for the accuracy, completeness, or usefulness of any information, apparatus, product, or process disclosed, or represents that its use would not infringe privately owned rights. Reference herein to any specific commercial product, process, or service by trade name, trademark, manufacturer, or otherwise does not necessarily constitute or imply its endorsement, recommendation, or favoring by the United States Government or any agency thereof. The views and opinions of authors expressed herein do not necessarily state or reflect those of the United States Government or any agency thereof. The work of OLM is partially supported by the French Agence Nationale pour la Recherche (Project ANR-2010-Blan-0904) and the GNR MoMaS funded by Andra, Brgm, Cea, Edf, and Irsn.

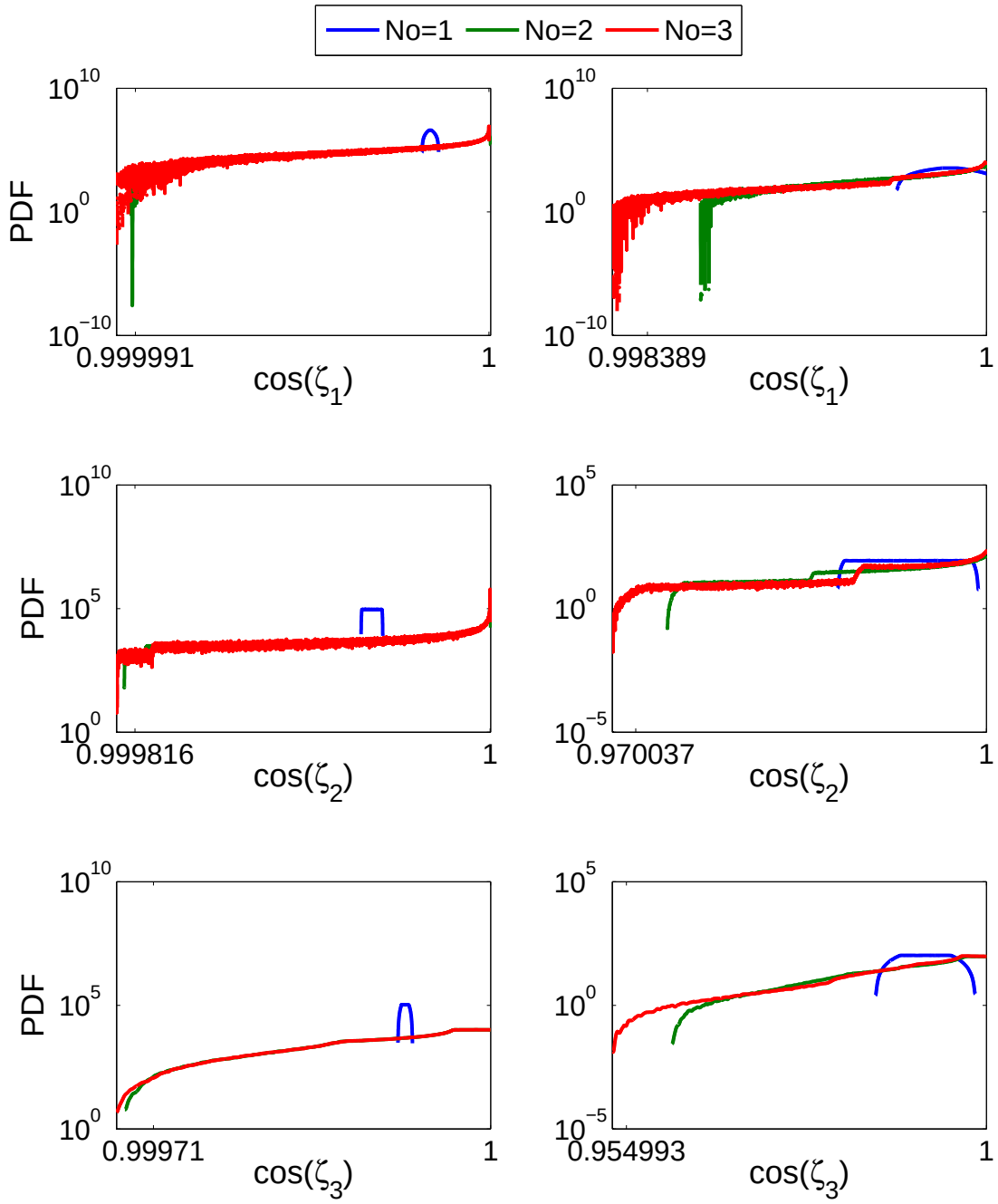


Figure 5: PDFs of $\cos(\zeta_i)$ at time $t = 0$. The left column corresponds to $\nu_1 = \nu_2 = \nu_3 = 0.02$ and $\nu_4 = 1$, and the right columns corresponds to $\nu_1 = \nu_2 = \nu_3 = 0.2$ and $\nu_4 = 10$. The curves are generated using NISP with 10 Gauss quadrature points and different expansion orders, $No$, as indicated.

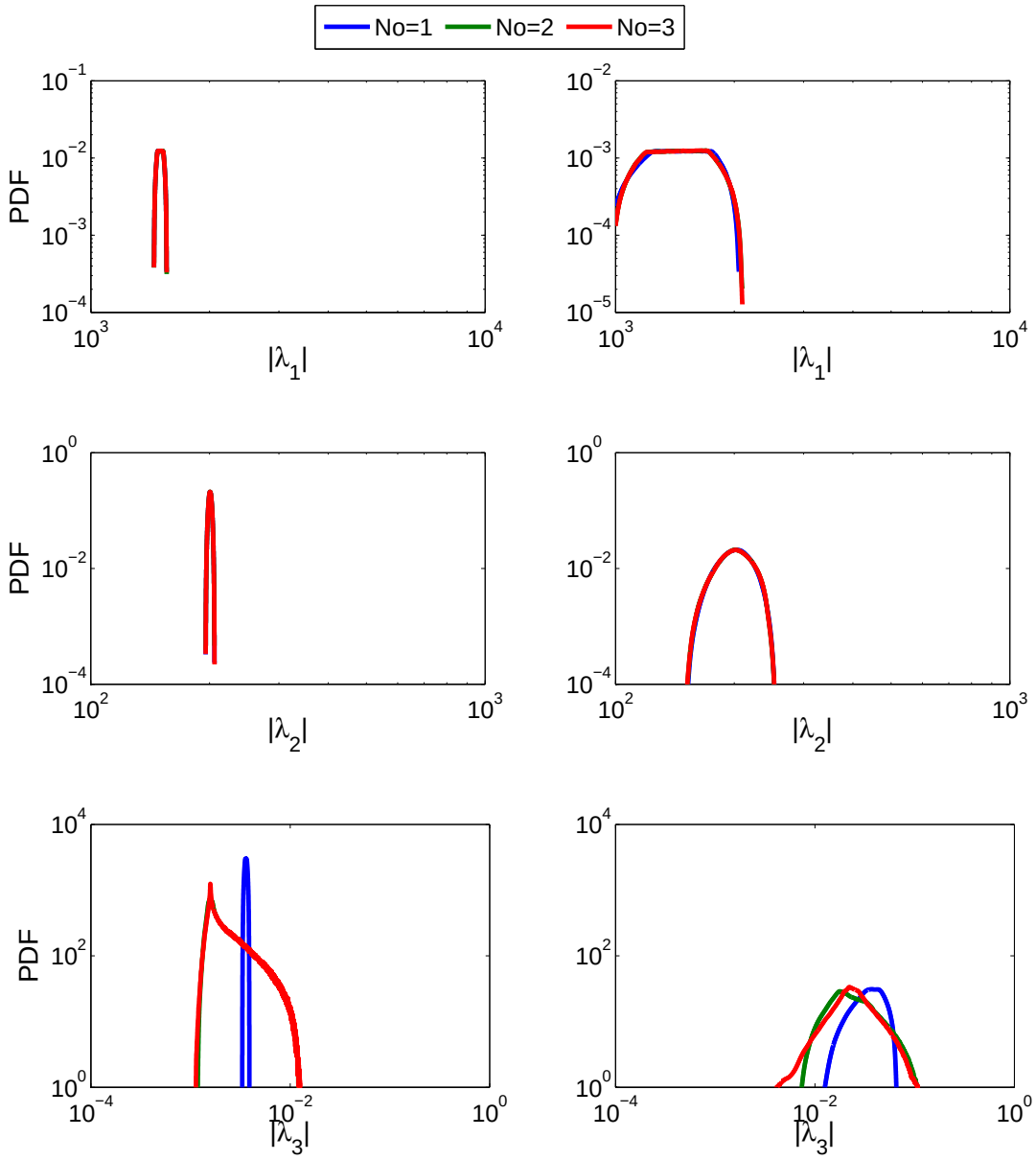


Figure 6: PDFs of $|\lambda_i|$ at time $t = 0$. The left column corresponds to $\nu_1 = \nu_2 = \nu_3 = 0.02$ and $\nu_4 = 1$, and the right columns corresponds to $\nu_1 = \nu_2 = \nu_3 = 0.2$ and $\nu_4 = 10$. The curves are generated using NISP with 10 Gauss quadrature points and different expansion orders, $No$, as indicated.

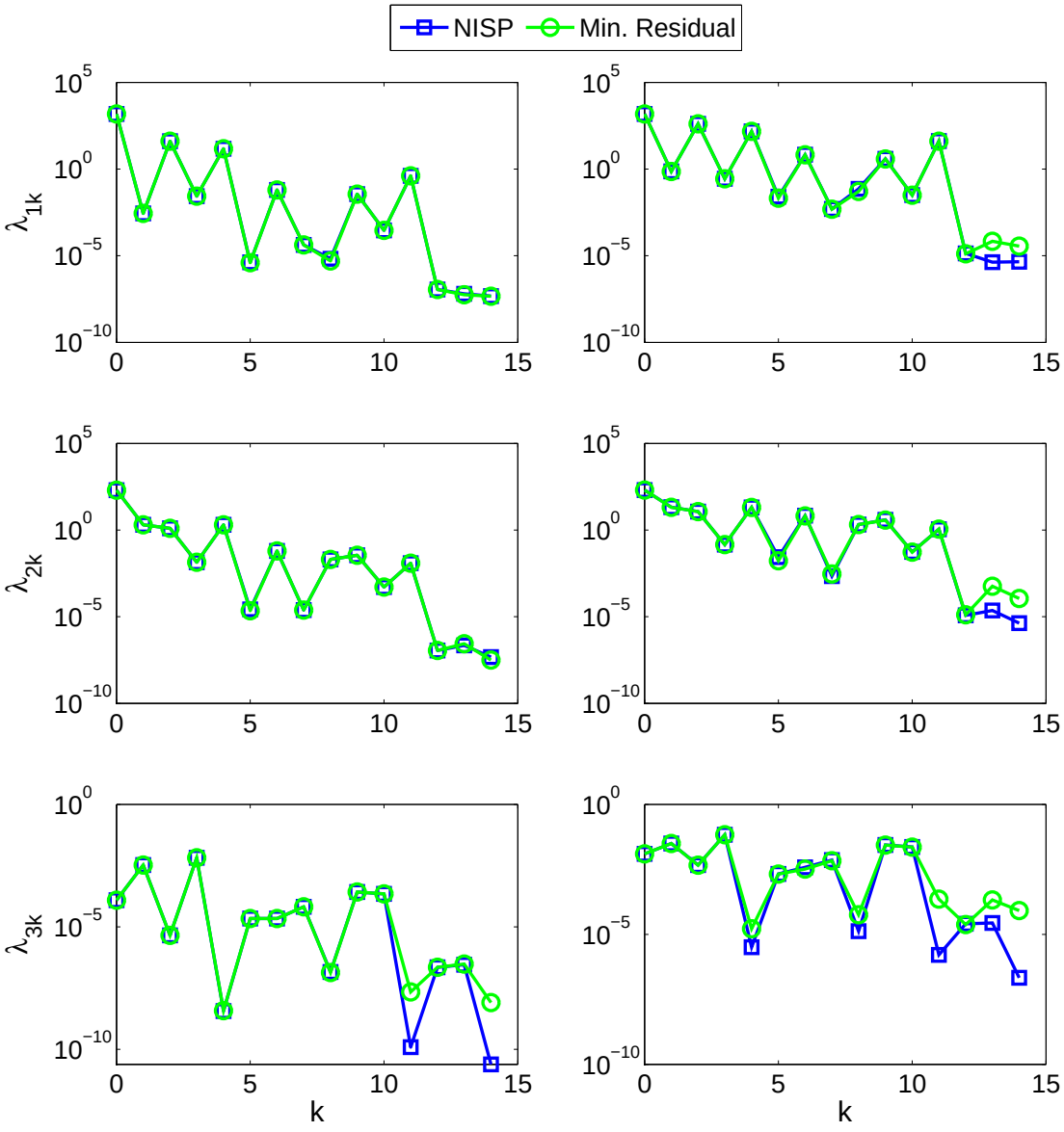


Figure 7: Spectrum of $\lambda_i$ (in absolute value) at $t = 0$. Left: $\nu_1 = \nu_2 = \nu_3 = 0.02$ and $\nu_4 = 1$; right: $\nu_1 = \nu_2 = \nu_3 = 0.2$ and $\nu_4 = 10$. Curves are generated using NISP with $No = 2$ and 10 Gauss quadrature points (blue), and using the residual minimization approach of Ghanem and Ghosh [9] (green).

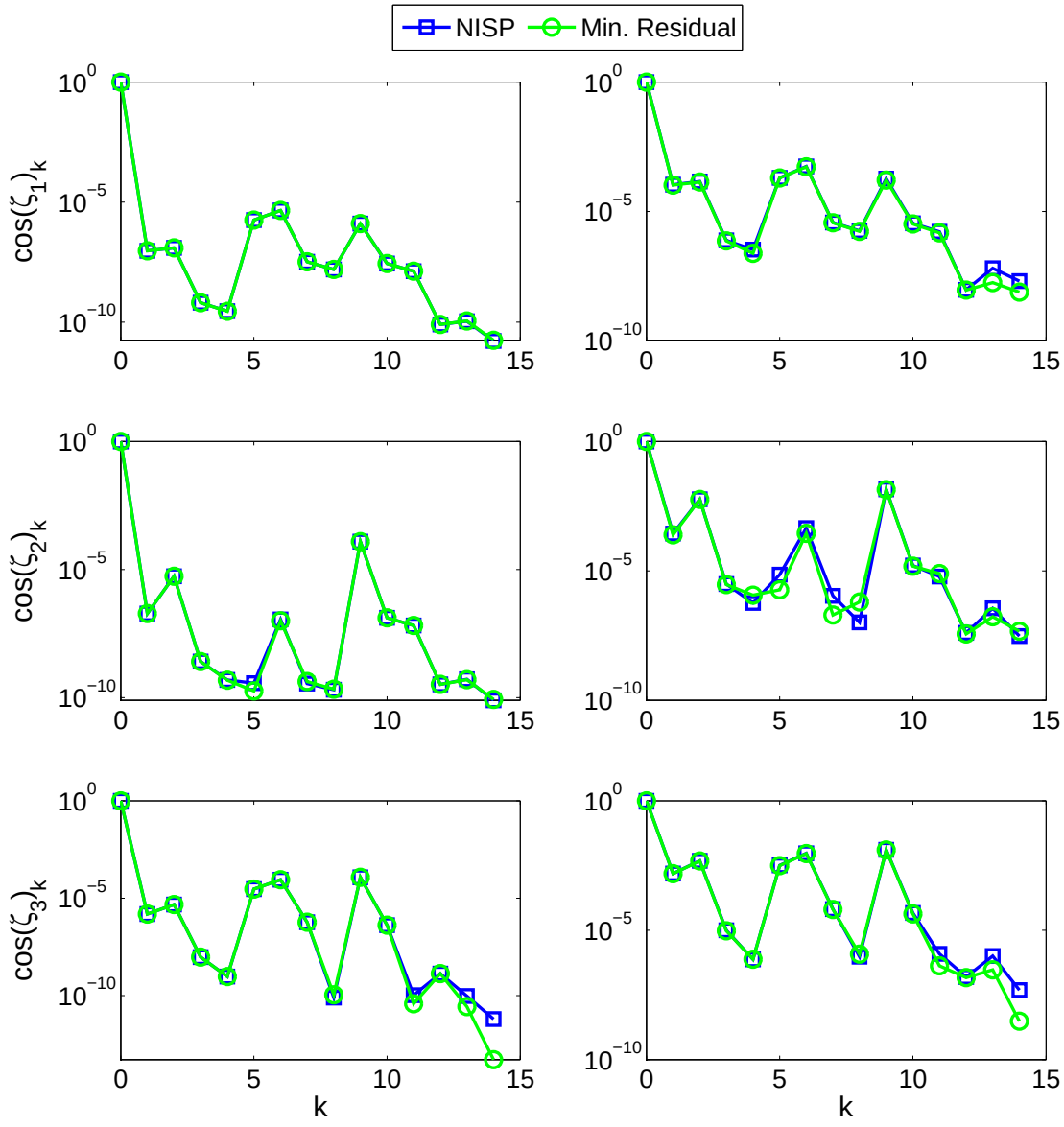


Figure 8: Spectrum of $\cos(\zeta_i)$ at $t = 0$. Left: $\nu_1 = \nu_2 = \nu_3 = 0.02$ and $\nu_4 = 1$; right: $\nu_1 = \nu_2 = \nu_3 = 0.2$ and $\nu_4 = 10$. Curves are generated using NISP with $No = 2$ and 10 Gauss quadrature points (blue), and using the residual minimization approach of Ghanem and Ghosh [9] (green).

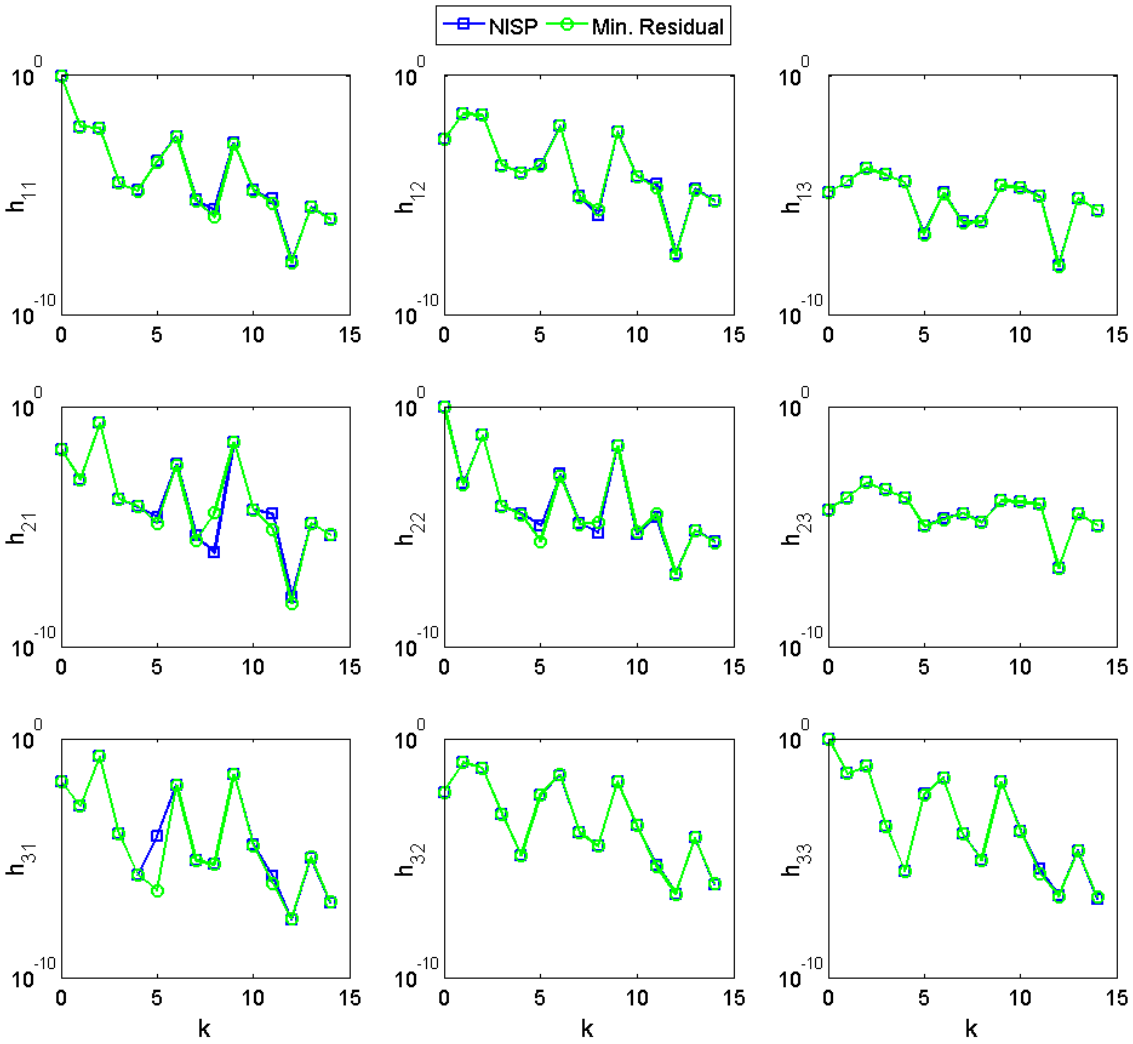


Figure 9: The spectrum of the coefficients $h_{ij}$ computed at time $t = 0$. Plotted are curves generated using NISP with $No = 2$ and 10 Gauss quadrature points (blue), and using the residual minimization approach of Ghanem and Ghosh [9] (green). The results are generated using $\nu_1 = \nu_2 = \nu_3 = 0.2$ and $\nu_4 = 10$.

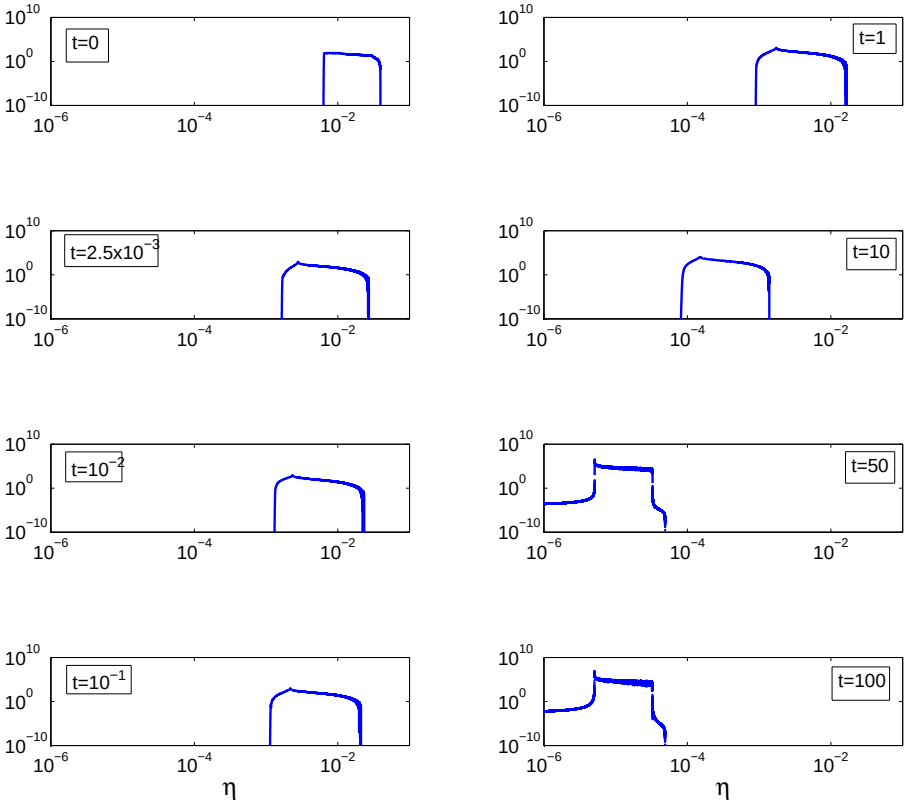


Figure 10: Evolution of the PDFs of $\eta$ computed for $\nu_1 = \nu_2 = \nu_3 = 0.02$ and $\nu_4 = 1$. The results are obtained using a second order PC expansion with spectral coefficients computed via NISP.

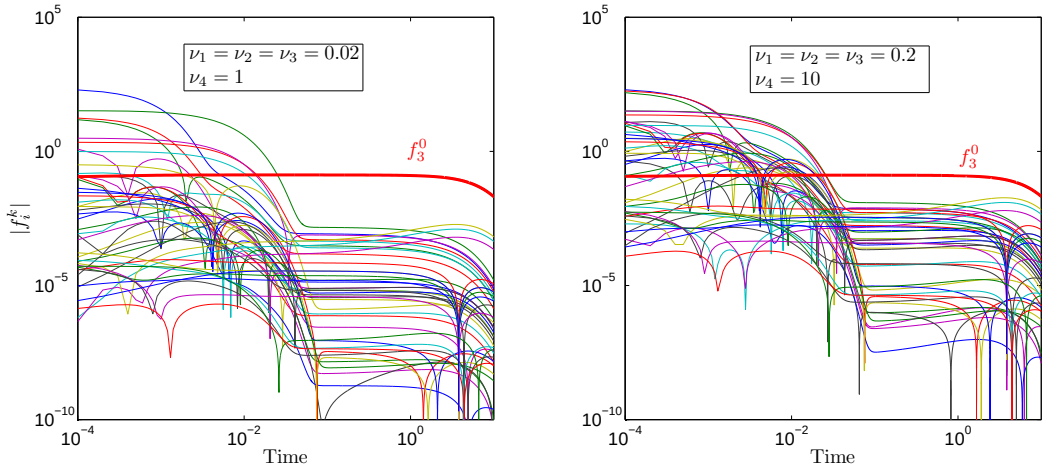


Figure 11: Evolution of the modes amplitudes $\left|f_i^k\right|$ of the Galerkin system with $No = 2$. The expanded ODE system model (48) is integrated using an explicit first-order scheme with $\Delta t = 10^{-4}$. Shown are plots generated for two different levels of uncertainty, as indicated.

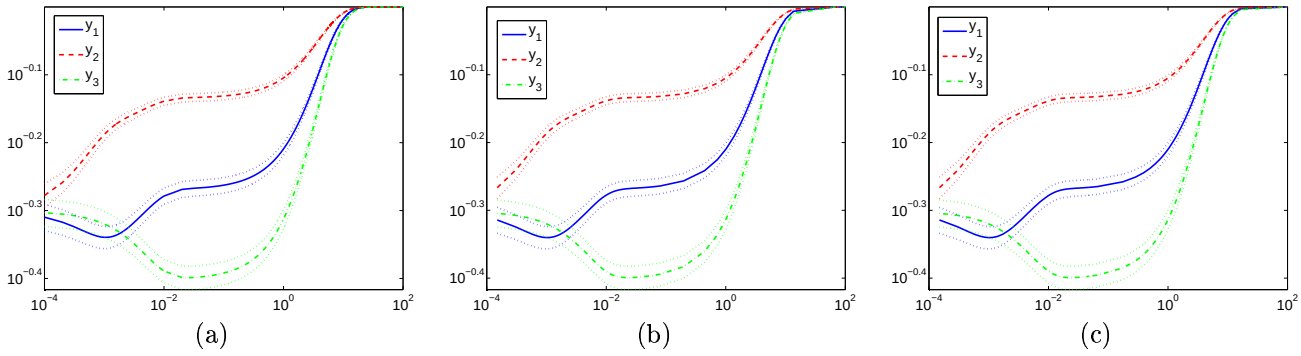


Figure 12: Random system trajectory computed using (a) explicit integration of the Galerkin system, (b) CSP with stochastic eigenvectors, and (c) CSP with nominal eigenvectors. The dotted lines show two standared deviation bounds. In all cases, the simulations are performed using $\nu_1 = \nu_2 = \nu_3 = 0.02$ and $\nu_4 = 1$.

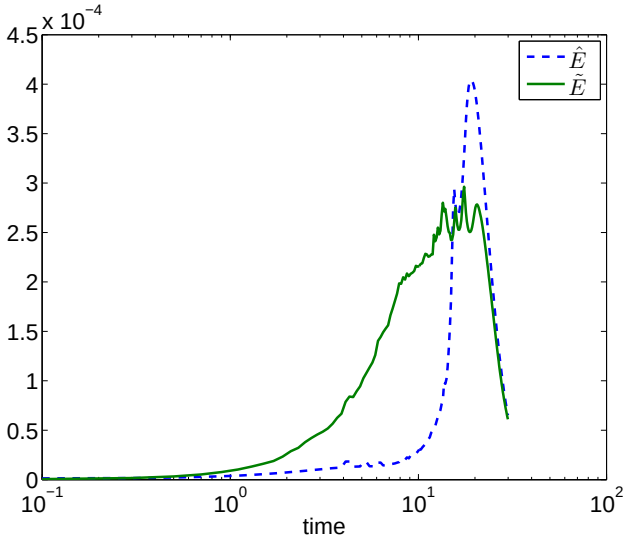


Figure 13: Relative error between the explicit Galerkin solution (with a second order PC expansion) and the CSP solutions. Results correspond to $\nu_1 = \nu_2 = \nu_3 = 0.02$ and $\nu_4 = 1$.